MODELING LAHARS USING TITAN2D FOR THE SOUTHERN DRAINAGE OF VOLCÁN COTOPAXI: IMPACT ON THE CITY OF LATACUNGA

By

Rebecca Williams
1st September 2006

A thesis submitted to the
Faculty of the Graduate School of
the State University of New York at Buffalo
in partial fulfillment of the requirements for the
degree of

Master of Science

Department of Geology

Acknowledgements

I would like to thank Dr M. Sheridan for the guidance, support and inspiration he has given to me over the course of the last two years.

Thank you to Dr M. Bursik and Dr C. Renschler for all advice and kind words.

To K. Dalbey and Dr A. Patra I remain indebted for all the help they provided with Titan2D.

Logistical support was provided by the Instituto Geofísico, Quito for the fieldwork.

Thank you to P. Mothes and Dr M. Hall for sharing their knowledge on Volcán Cotopaxi.

Thank you also to Mayor Oswaldo Navas Ramos for providing data and information about Latacunga and Defensa Civil.

Pablo Samaniego, Diego Barba and Daniel Andrade V. of the Instituto Geofísico, Quito provided data from the seismic and AFM instruments, and from preliminary fieldwork for Chapter 3. I gratefully acknowledge the assistance of Mario Guzman with the GPS surveying in July 2005.

Funding was provided by NSF grants EAR-0087665, EAR-0439093, ITR-0121254 to M.F. Sheridan.

Thank you to all of those at UB, both the Department of Geology and the Tae Kwon Do team for making it fun. To Bettina and Jorge, my family away from home, I thank you with all my heart. Most of all, I would like to thank Adam Stinton for all his love and support from the last two years. I couldn't have done it without you.

Contents

List of Figures

List of Tables

Foreword

This research is centered on assessing the impacts of lahars on the city of Latacunga, Ecuador using the Titan2D model and comprises the main bulk of this thesis. It should be noted that Chapter 3 consists of a distinct research project which describes the model and provides a field evaluation so that confidence can be placed in the results of the thesis study. Chapter 3 was co-authored with A. J. Stinton and M. F. Sheridan and is to be submitted to the Journal of Geothermal and Volcanological Research.

Abstract

Lahars triggered by mobilization of deposits from volcanic explosions have occurred at Volcán Cotopaxi, Ecuador on the average of once every century over the last two millennia. Lahars from Cotopaxi may flow down three main drainages, impacting a present day population of around 3 million inhabitants. Río Cutuchi, the main drainage to the south of Cotopaxi, headwaters on the flanks of Rumiñahui and Cotopaxi Volcanoes. This river flows southwards through several communities, including the city of Latacunga (population 52,000). Its path is generally parallel to the Pan American highway. Many small scale lahars have followed this drainage, as well as some large scale historical flows, such as the great 1877 debris flow that severely impacted the population along the Río Cutuchi. This study used the Titan2D model to simulate lahars of various volumes that correspond to actual deposits along the Río Cutuchi in the vicinity of Latacunga. The purpose was to investigate the hazard that lahars might present to the current population should Cotopaxi become active again and produce debris flows. The study area is restricted to the region adjacent to Latacunga where detailed field data are compared with the model results. Simulations utilized topographic, stratigraphic, and historical inundation data collected in the field in the summer of 2005 to determine probabilistic lahar inundation zones for the debris flows of various sizes. These inundation zones have been analyzed in conjunction with infrastructure data for Latacunga so that the impact of various scale lahars on the city can be assessed.

Chapter 1 Introduction

1. Introduction

Lahars, or volcanic debris flows, are high-sediment concentration flows that occur on volcanic terrains. They may be a primary phenomenon that occurs during an eruption or less predictably, a post-eruptive phenomenon or even unrelated to an eruption. Lahar formation requires an adequate water source, an abundant unconsolidated debris supply, steep slopes and substantial relief, and a triggering mechanism (Vallance, 2000). Lahars may be initiated by torrential rains, or rapid melting of snow or ice caps on the volcano's peak. They can also form by flank collapse of large volcanoes if there is sufficient pore or hydrothermal water available.

Lahars are particularly dangerous to communities near volcanoes. As the flows of sediment and water travel down the volcano flanks, they incorporate a large quantity of sediment and rock fragments, making lahars very destructive. These gravity driven flows descend valleys, but their large volume enables them to overflow their banks to cover lateral areas of low gradient. This results in distal communities being unexpectedly inundated, sometimes with catastrophic consequences.

Previous catastrophic lahars have been well documented; for example the mudflow at Nevado Del Ruiz, Colombia in 1985 (Voight, 1988; Pierson et al., 1990; Tanguy et al., 1998,) and lahars following the eruption of Mt. Pinatubo, Philippines in 1991 (Pierson et al., 1992; Rodolfo, 1989; Arboleda and Martinez 1996).

The common occurrence of lahars and their effects on volcanic communities demonstrate the need to consider the hazards on individual drainage systems for specific volcanoes. In this way, accurate inundation zones and hazard maps can be generated so that catastrophic events can be reduced. This study will concentrate on a portion of the Río Cutuchi drainage system on the south flanks of Volcán Cotopaxi, Ecuador. This area contains many communities, some of which are situated on terraces formed by lahars in recent geological history. Potential lahars are simulated using the two-phase Titan2D model (Pitman and Le, 2005) to create a probabilistic study of inundation areas for the city of Latacunga, Ecuador.

1.1 Background on Volcán Cotopaxi

Cotopaxi is one of the highest active volcanoes on earth with a summit elevation of 5911 m (Global Volcanism Program, 2005) and is considered to be Ecuador's most dangerous. It is a composite volcano with 3000 m of relief. Its upper flanks have slopes of around 25-30˚ and their snow and ice fields cover approximately 20 km^2 with a volume of 1.0 km^3 (Mothes et al., 1998) (present day glacier seen in Figure 1). The lower flanks are incised by valleys forming three main drainages: to the north the Ríos Pita and Esmeraldas, to the southwest the Río Cutuchi and Pastaza and the Río Tambo and Tamboyacu-Napo to the east. The volcano's eruptive history began around 0.5 Ma ago, dominated by rhyolitic magmatism. The current andesitic phase of volcanism began around 4100 years ago, resulting in the present cone (Mothes, 2006).

1.1.1 Recent Activity

Recent activity produced plinian eruptions and associated small volume pyroclastic flows and surges (Barberi et al., 1995). Such activity resulted in the melting of the summit ice

Figure 1: Summit glacier of Volcán Cotopaxi, Climbing Refugio (yellow building) for scale.

and snow caps producing mudflows. Barberi et al. (1995) have estimated that Cotopaxi experienced an average recurrence of one explosive, lahar-triggering event every 117 years over the last two millennia. Activity at Volcán Cotopaxi is summarized in Table 1.

1.1.2 Lahar Activity

Two types of lahar occur commonly at Volcán Cotopaxi (Andrade et al., 2005). Primary lahars are those generated from pyroclastic flows and the melting of the volcano's ice cap. Secondary lahars occur when heavy rains remobilize ash deposits following an eruption. The Río Cutuchi has experienced primary lahars in 4500 yrs BP and in the years 1742, 1743, 1744, 1766, 1768, 1855 and 1877 AD.

Age	Principal Eruptions	Sub-plinian - plinian tephra falls	Pyroclastic Flows	Lahars	Lava Flows	VEI
1880 AD	1	1				2-3
1877	2	1	yes	many	yes	4
1853 - 1854	2	1	yes	many	1	3-4
1768	1	1	yes	many	1?	4
1766	1	1	yes	many		3
1744	1	1	yes	many		4
1743	1	1	yes	many		3-4
1742	3	2	yes	2 groups		4
1532 -34	2	2	yes	2 groups	1	3-4
900 yBp	4	3	yes	many		3-4
1000 yBp	2	2	yes	2 groups		>4
1180 yBp	1	1	yes	many		3-4
1210 yBp	1	1	yes	2 groups	1	4
1770 yBP	1	1	?	many	several	4
1880 yBP	1	1	yes	2 groups	1	>4
1880-2000 yBP	1	1	yes	many		4
~2000 yBP	1	1	yes	?		4
TOTAL	26	22	>14 times	>20 times	>7 times	

Table 1: Summary of recent activity. (Mothes, 2006).

The enormous Chillos Valley lahar (CVL) was an ash-flow generated debris flow from Volcán Cotopaxi that formed about 4500 years BP. The CVL was generated by a rhyolitic ash flow that followed a small sector collapse on the north and northeast sides of Cotopaxi (Mothes et al., 1998). This flow melted part of the volcano's ice caps and the torrents transformed into a debris flow on the flanks. The lahar descended river systems on the N-NE flanks and flowed as far as the Pacific Ocean, 326 km from the volcano.

Flows also reached over 130 km east into the Amazon Basin. Although the larger portion of the CVL flowed down the northern drainages the smaller, southern portion still devastated a wide swath (Figure 2). Once the CVL filled the deep canyons of the Río Cutuchi, the flow spread as it passed downstream and into the Latacunga Valley. Here, the flow widths reached 3-5 km beyond its channel walls, over a 25 km stretch with depths of 20 m (Mothes et al., 1998). The flow extended downstream beyond Latacunga, flooding 160 km^2 from the Latacunga Valley down to Panzaleo. The overall volume of the CVL is estimated to be around 3.8 km^3 (Mothes et al., 1998).

The Chillos Valley Lahar is not typical of the recent activity at Cotopaxi. Historical events are characterized by smaller eruptions with scoria flows that melt the glacier creating lahars. Near the volcano, lahar deposits are dark grey, clast-supported, well-packed breccias, with a thickness of 1-3 meters (Mothes, 2006). They may include blocks up to 8 m across; however, it is more common to see clasts in the range of 2-20 cm (Mothes, 2006). Most clasts are andesitic, possibly fragments of fresh lava blocks and some scoria. Hyperconcentrated stream-flow deposits occur in distal areas of the drainage system.

In 1742 there were three eruptions which produced lahars that caused destruction to haciendas, livestock, and people in the Latacunga Valley (Mothes, 1991). Similarly, eruptions in 1766 and 1768 created lahars that inundated major drainages, causing damage to local communities. The last catastrophic eruption of Volcán Cotopaxi occurred in 1877. This eruption and its associated lahar, which caused widespread

damage and the deaths of over 300 people (Major and Newhall, 1989), are discussed in detail in Chapter 2 as it is considered the eruption scenario for future events.

Many communities surrounding Cotopaxi are built on deposits from the CVL and other lahars and are at great risk from future flow**s.**

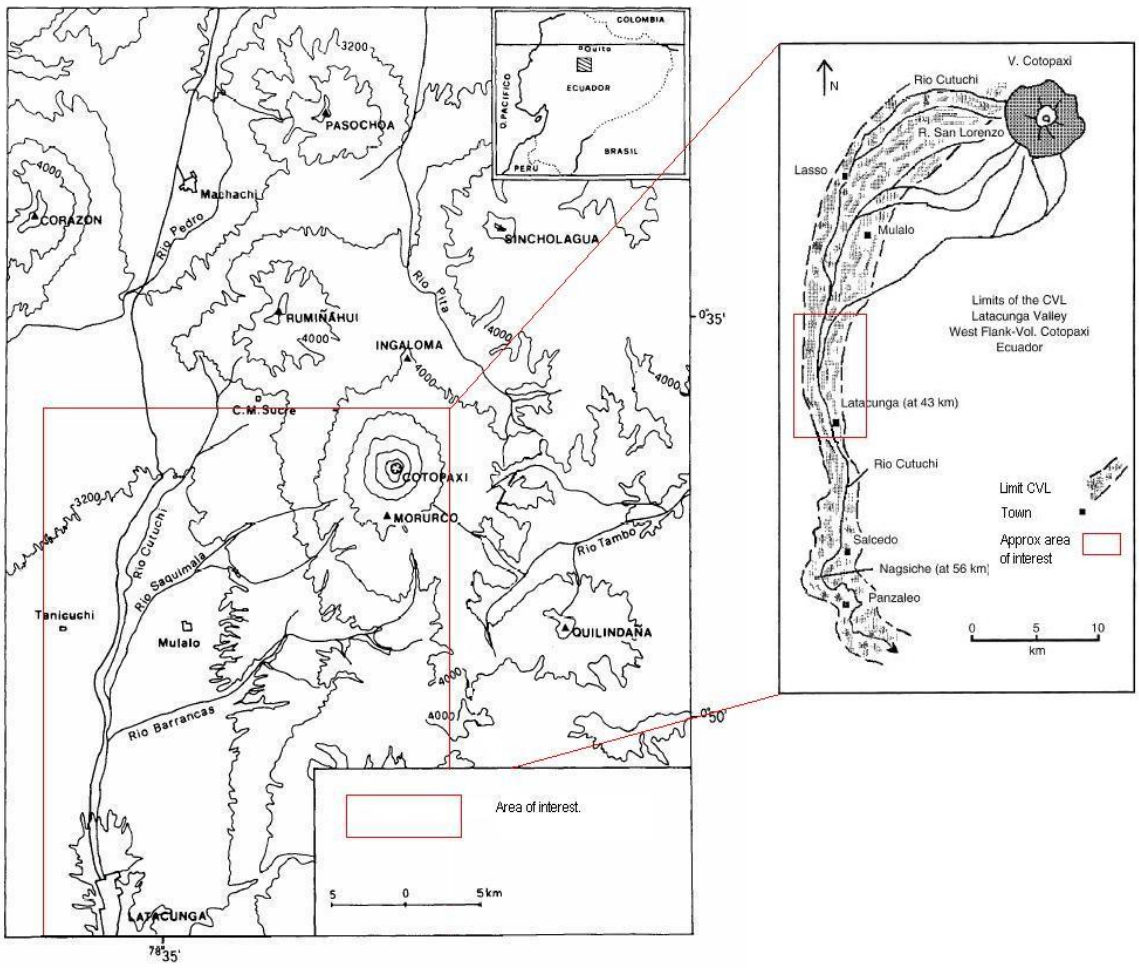

Figure 2: Topographic map showing Cotopaxi, the Río Cutuchi and Latacunga (adapted from Barberi et al., 1995) and magnified section showing map of Latacunga Valley and the major streams draining the southwest side of Cotopaxi to form the Río Cutuchi. The extent of the CVL deposits are shown. (adapted from Mothes et al., 1998).

1.1.3 Current Activity

January 2001 saw renewed activity at Volcán Cotopaxi (Molina et al., 2006). Long-period (LP) seismic events increased, followed by a swarm of tremors in November. In June of 2002 very long-period (VLP) events accompanied the LP signals, which began to occur directly under the volcano. Temporal changes between the VLP and LP events continued until September 2003 when the VLP signal disappeared leaving the LP signal to dominate. Rivero et al., (2006) proposed that injections of new magma occurred in March 2003, Oct 2004 and April-May 2005 indicated by increased fumarolic activity at the summit. Activity at Cotopaxi is also suggested by a thermal anomaly (Ramon et al., 2006.). This renewed activity has led scientists to consider the possibility of an eruption and what that might mean for the large population now living in Cotopaxi's shadow. This study has arisen out of a need to consider a variety of eruption scenarios in light of the recent activity and the large population centers along the main drainages of the volcano.

1.2 The Río Cutuchi

The Río Cutuchi is the river system considered for this study. It is the principle river southwest of Cotopaxi (see Figure 3). Its headwaters are in the south of Rumiñahui (Figure 3), a heavily eroded dormant volcano to the west of Cotopaxi and has tributaries covering the entire west flanks of Volcán Cotopaxi. Mothes et al. (1995) state that historical accounts and stratigraphic studies show that the majority of the small debris flows from Cotopaxi since 1532 flowed down the west and southwest tributaries of the Río Cutuchi.

The source region for the Río Cutuchi has been continuously blanketed by tephra falls from eruptive activity of Cotopaxi over the last 2000 years (Barberi et al., 1995). These deposits supply the loose debris for lahar flow generation. As previously mentioned, Cotopaxi has abundant summit ice and snow caps which would supply the water source needed for lahar generation. It is feared that torrential rain or rapid melting of these ice caps will cause mobilization of the unconsolidated debris and once again lahars, in the source region of the Río Cutuchi.

The Ríos Pita and Cutuchi flow southward along the 50 km wide Inter-Andean Valley. The towns and cities within this area have been severely affected by lahars from Cotopaxi on several occasions since the arrival of the Spanish Conquistadors in 1532 (Mothes et al., 1998). Many towns are built upon the CVL deposits (Figure 1), and even younger terraces. Latacunga alone is home to around 52,000 people (Censos 2001). Apart from cities and people, the infrastructure of the area is also at risk. The Pan-American Highway runs alongside the Río Cutuchi in many places and a large lahar could cause damage to this major road.

1.3 The City of Latacunga

Latacunga is the principle city in Cotopaxi Province. It is a sprawling town that is the economic centre for the surrounding towns and villages. The official population currently stands at around 52,000 people. It is the location for the regions principal hospitals, police force, markets and is also home to the Civil Defense for the Cotopaxi Province. This city, as previously mentioned, is also built on the banks and into the

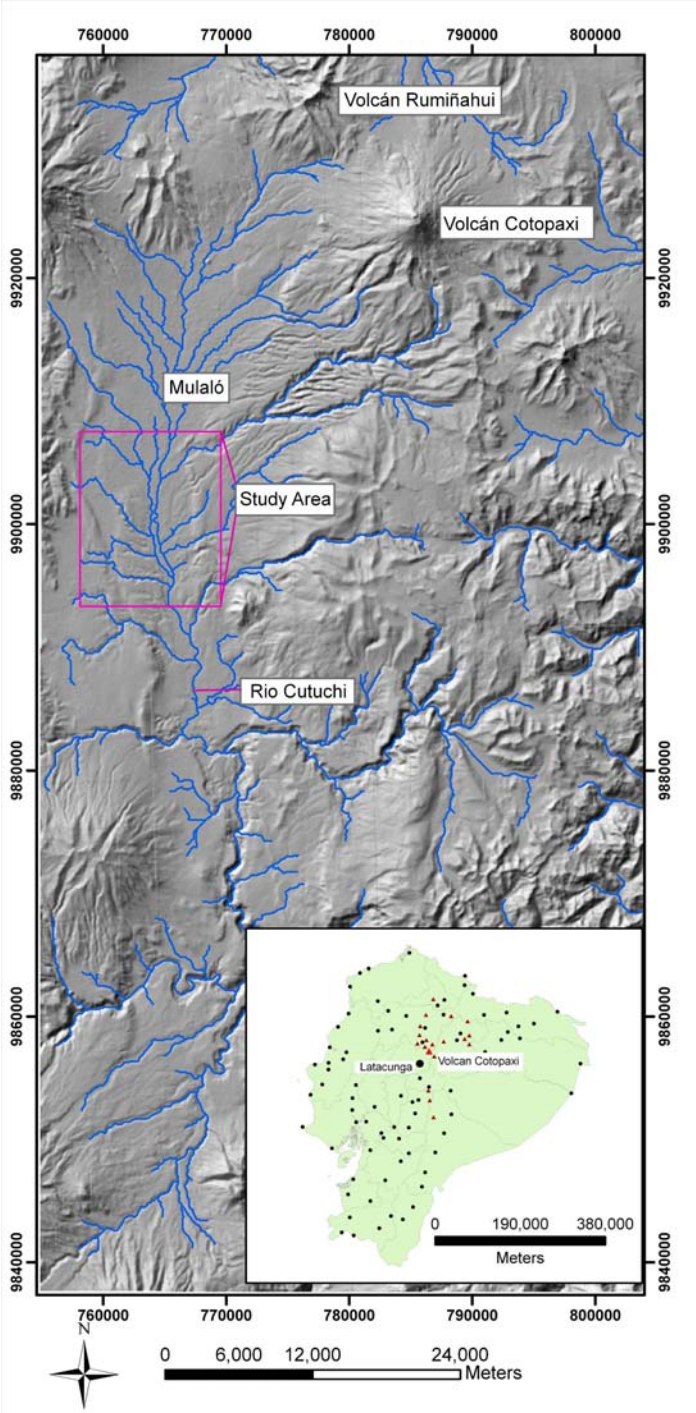

Figure 3: Location of Volcán Cotopaxi, the Río Cutuchi and the study area (highlighted with pink box). The inset shows the geographical location of Volcán Cotopaxi and Latacunga in Ecuador.

channel of the Río Cutuchi (Figure 4). Historically, the city has been destroyed five times by lahars and suffered heavily in the 1877 event, as discussed in Chapter 2. It is located 60 – 70 km from the volcano summit.

Figure 4: Left) The city of Latacunga with the Río Cutuchi channel in the foreground and Volcán Cotopaxi in the background. Right) Building within the channel limits.

1.4 Objectives and Purpose of the Study

This study evaluates the potential effects of lahars on the city of Latacunga in the event of a future eruption of Cotopaxi Volcano. The study uses a new modeling technique, the two-phase Titan2D model, to simulate potential lahars in the Rio Cutuchi to create probability maps of lahar inundation. These maps are used to consider the detailed effect a potential lahar would have on the vital resources and lifelines of the city. This is a scientific analysis using a computational model that has inherent uncertainties. It is not a

professional planning or risk document but may serve as an example for those who have these types of responsibilities.

This study also presents an evaluation of the two-phase Titan2D model. Comparisons are made between observations from an actual lahar that occurred in February 2005 and simulations of this flow. The study area chosen for this evaluation is the Vazcún Valley at Volcán Tungurahua, Ecuador. This example was chosen for the fine resolution 5m DEM that was created using GPS data and the opportunity to make detailed observations of inundation area and flow height in the field.

Chapter 2 The 1877 Lahar

2. The 1887 Lahar

The 1877 eruption has been chronicled by Sodiro (1877) and Wolf (1878) and has been extensively studied by several groups (Barberi et al., 1992; Aguilera et al., 2004; Mothes 1991, 2006). A series of strong detonations started the event at 10 am on June 26th. A plume of gas and ash rose above the volcano associated by a rain of ash and pyroclastic flows described by Wolf (1878) as "a potful of boiling rice which began to pour out" of the crater. This has been interpreted as a 'boiling over' scoria flow rather than a pyroclastic flow that occurred due to column collapse. The eruption is considered to be of magnitude VEI 4 (Mothes, 2006). These flows traveled over the ice cap, including the western drainage ice cap which is thought to have had an area of 5.3 km^2 and a volume of 0.260 km^3 (Mothes, 2006). This triggered large floods along all three main drainages, which beyond the glacier mixed with pyroclastic and ice blocks causing intense erosion and gullying, rapidly evolving the flood into debris flows (Aguilera et al., 2004).

2.1 Flow Characteristics

The flows are estimated to have had discharges of 50,000 – 60,000 m^{3}s^{-1} with velocities in excess of 20 ms^{-1} (Mothes, 2006). Sodiro (1877) noted that "the road between Mulaló and Latacunga was full of travelers, and given the great velocity of the lahar, many people, some on galloping horses, were overcome by the advancing wave, and thus disappeared". Lahar heights have been estimated to be up to 35-40 m (Mothes, 2006) although eye witness accounts give heights closer to 50 m (Sodiro, 1877) and 100 m (Wolf, 1878).

2.2 Lahar Effects

The lahar caused devastation in the Chillos and Latacunga valleys destroying textile factories, haciendas, towns, bridges and indigenous communities. Wolf (1878) was so moved by the events that he wrote "…on this terrible day hundreds of people and thousands of animals lost their lives and Cotopaxi changed the countryside into deserts of sand and stones and destroyed in one hour the work of many generations". This barren landscape described by Wolf is still evident today in the area around Mulaló (Figure 3). Here, fields strewn with boulders remain unfarmed due to the poor quality of the land. Some attempt has been made to grow eucalyptus trees, with little success (Figure 5).

The lahar that flowed down the volcano's north flank arrived at the port of Esmeraldas on the Pacific coast some 18 hours later carrying within it "cadavers and pieces of houses and furniture from the Chillos Valley". The lahar that traveled down the southern drainages reached the city of Latacunga, some 43 kilometers from the crater, in less than an hour (Barberi et al., 1992).

At the north of Latacunga the three-story textile factory, located on the east bank of the Río Cutuchi, was buried by deposits (Figure 6). This site has been excavated and was covered in some "seven meters of volcanic mud and sand" and debris including lahar encased machinery, masonry and the remains of a 7 or 8 year old boy (Museum of the Central Bank of the Equator). This site provided the excellent exposures of the 1877 lahar deposit, as discussed later in this chapter.

Figure 5: Debris Fan north of Mulaló. Note the barren landscape and the abundant boulders from the 1877 lahar.

2.3 Lahar Deposits

Deposits near the volcano, in the Mulaló (Figure 3) region, are characterized by a base of ashfall/lapilli/pumice marker beds, with an overlying debris flow deposit with no bedding, although some breaks in the deposit are visible. Ceramics are common at the base of the flow which mainly consists of polylithic clasts that are sub-angular to sub-rounded. Red scoria clasts are common in the 1877 deposits, which tend to be the upper most unit in much of the Latacunga Valley.

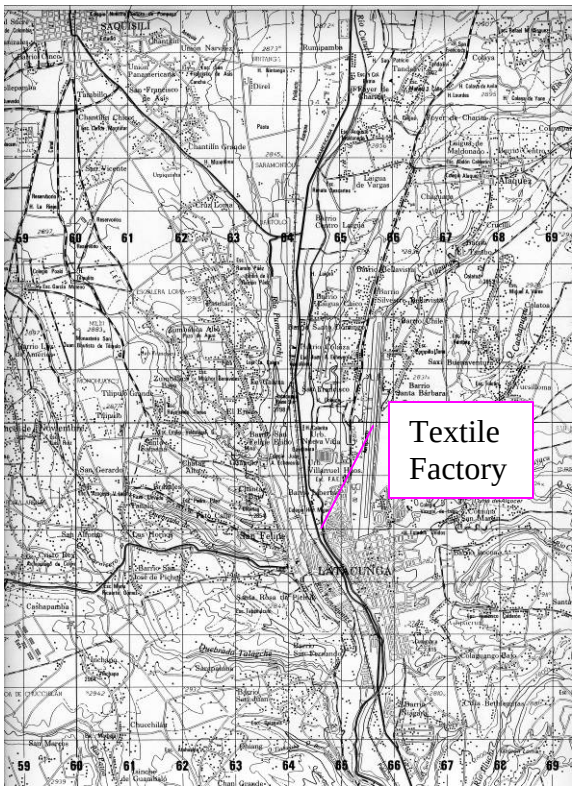

Figure 6: Excavated remains of the textile factory buried by the 1877 lahar. The location of the textile factory is shows in adjacent topographic map. This is the location of the two stratigraphic columns seen in figure 7.

At the textile factory site in Latacunga, the main unit in the deposit tends to be poorly sorted, clast-supported with a pale brown, fine sand matrix (Figure 7). It is polylithic with an abundance of large red scoria clasts and black lithic (juvenile?) clasts which range from sub centimeter to 20 cm in size. Ceramic tiles occur within the deposit (Figure 8a) as well as some boulders which reach up to 60 cm in size. The second unit is similar but has a smaller range of clast sizes (<10 cm). The third unit seen here is a

matrix supported, sandy unit with some normal grading. The fourth unit is a very fine grain, laminated unit that is fairly unconsolidated.

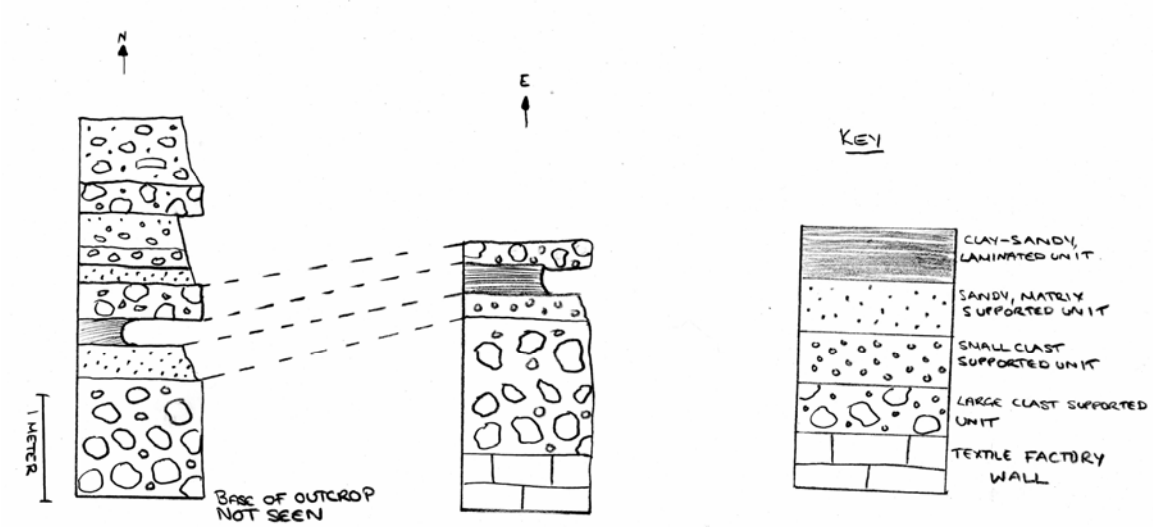

Figure 7: Basic stratigraphic column of two sections seen at textile factory; for location see figure 6. These sections are located adjacent to each other in the excavated section (figure 8), the south facing section is seen in fig 8b and the west facing section is adjacent to it, in the egde of fig 8b. Note the inconsistency of the deposit, which may be a factor of the flow interacting with walls, rooms and other features of the factory

These deposits show different pulses of flow, indicating that the flow was not steady but had several waves. The very fine, laminated units could be from 'swashing' of a watery flow within the building (Figure 8c). There is no imbrication seen in the deposit indicating that there was no internal shear. The majority of the clasts appeared to be eroded material, with little to no pumice or other juvenile 'source' material, indicating that the flow experienced extreme bulking. Whilst the textile factory presents well preserved sections (Figure 8b) that are obviously related to the 1877 event, the deposits seen here are likely to not be typical of the deposits from this event.

Figure 8: a) Red ceramic tile in lahar deposit. **b)** Section of deposit from textile wall (base of photo) to top (unknown if top of deposit), correlates to north facing stratigraphic column in Figure 7 c**)** Very fine, laminated units.

The flow will have interacted with the building, causing sorting, reworking and other atypical behaviors. Further downstream, the deposits show a transition from clast-rich debris flows to hyperconcentrated stream-flows (Mothes, 1991).

2.4 Previous work on the 1877 lahar.

The extent of the deposits for the 1877 lahar are the basis for the lahar hazard zone published in the *Mapa Regional de Peligros Volcanicos Potenciales del Volcán Cotopaxi – zona sur* (Hall et al., 2004). A VEI 4 eruption could produce an 1877 size lahar and is considered the typical eruption style for Volcán Cotopaxi (Andrade et al., 2005).

Some work has been made on numerical modeling 1877 size lahars for the northern and southern drainages (Barberi et al., 1992, Aguilera et al., 2004). Aguilera et al. (2004) modeled lahars with initial volumes of 35 - 80 x 10^6 m^3 for the northern drainages with

the 60 x 10^6 m^3 simulations reproducing the maximum heights attained by the lahar in this valley. Barberi et al. (1992) simulated flows with volumes of 45, 90 and 150 x 10^6 m^3 that reproduced maximum heights actually reached by the 1877 lahar.

2.4.1 Barberi et al., 1992: Reconstruction and numerical simulation of the 1877 lahar.

The numerical model employed in this study is based on mass and momentum balance laws for a channeled flow (Takahashi, 1978, 1980; Barberi et al., 1991; Macedonio & Pareschi, 1992). The equations assume a homogenous flow and constant volume. Input parameters are volume, solid concentration and topography. Topographic data is derived from digitizing cross sections with 1 km spacing from 1:25,000 and 1:50,000 topographic maps and from a field survey.

Barberi et al. 1992, made comparisons with 1985 Nevado Del Ruiz lahar, 1980 Mt St Helens lahar and the 1877 Cotopaxi lahar to infer hydrograph shapes which give information on volume of water and solid fraction. The size of the glacier was also taken into consideration for volume estimates, which came to be 45 x 10^6, 90 x 10^6 and 150 x 10^6 m^3, using a solid volume fraction of 70%. They concluded that the results showed that the numerical model was able to simulate the debris flow along a meandering valley successfully. Historical data was reproduced by the model such as lahar height, discharge, and arrival time. From this they concluded that an 1877-style lahar would strike Latacunga one and a half hours after lahar generation, with a 10 m high lahar wave with a maximum discharge of 9100 m^3s^{-1} (Figure 9).

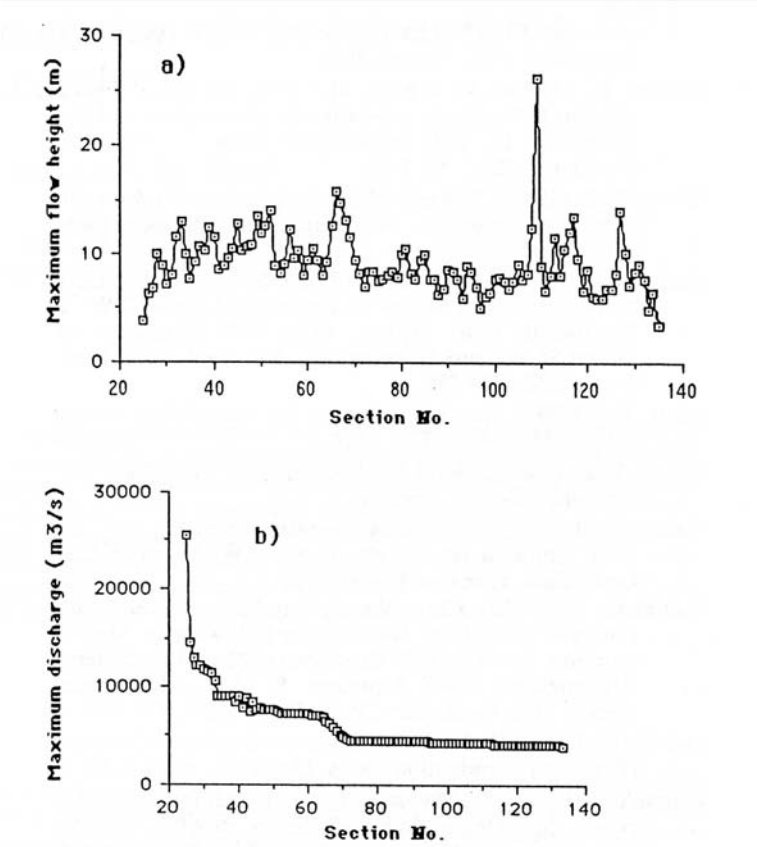

Figure 9: a) Maximum flow height and b) discharge along Río Cutuchi – Río Pastaza for a lahar being generated by an 1877-like eruption (from Barberi et al., 1992)

2.5 The possibility for an 1877-style event in the future.

Aguilera et al. (2004) and Barberi et al. (1992) discuss the probability of a recurrence of an 1877-style event. Both papers recognize that the volume of lahar is heavily dependent on glacier size, which has changed since the last event. Today's glaciers on Cotopaxi are generally considered to be 2/3 the size of the 1877 ice cap (Barberi et al., 1992; Aguilera et al., 2004). This would mean that the maximum potential lahars may be somewhat smaller than the 1877 lahar.

The second factor to consider is the recurrence probability of an 1877 size eruption. Barberi et al. (1992) used stratigraphic information (Barberi et al., 1995) from the last 2,000 years to consider a recurrence interval using the Poissonian probabilistic

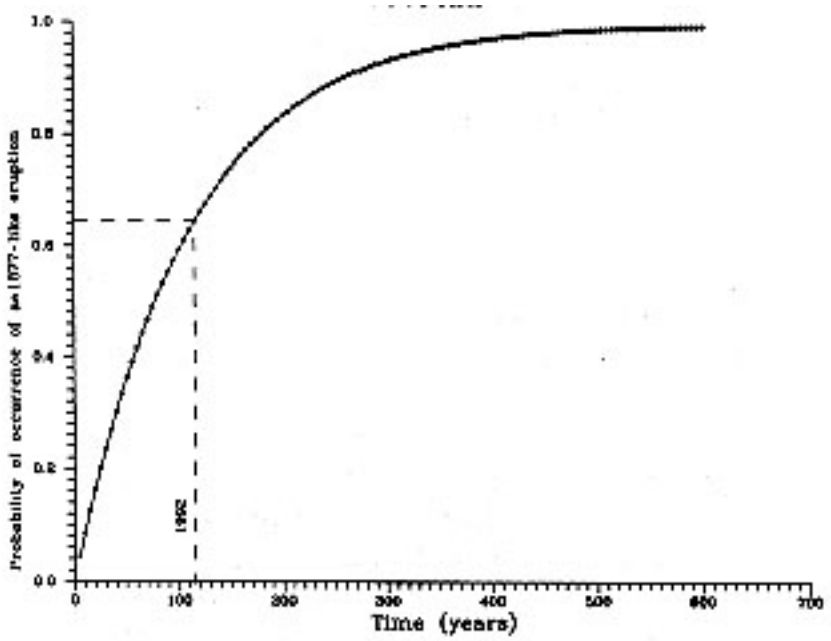

Figure 10: Probability of occurrence of an 1877 style eruption (From Barberi et al., 1992).

distribution of repose time (Equation 1; Wickmann, 1976).

$$P = 1 - \exp(-Te/Tr) \quad (1)$$

Where Te is the exposure time (repose) and Tr is the recurrence rate.

Figure 10 reports these results as the probability of eruption as a function of time. Using this information, the probability for recurrence of an 1877 size event occurring in 2006 is 0.64. The third factor to consider is not the probability of lahar generation, but of the effect a similar size lahar would have today. The population distribution in the 1877 Latacunga Valley was considerably different than it is today. In 1991 it was estimated

that 20,500 people lived in the zones of highest risks (Mothes, 1991) and that homes, new industries, hospitals, schools, the Pan American Highway and other infrastructures have been built on top of lahar deposits (Figure 11). Population expansion and building growth continues to occur in these zones today and into the channel itself (Figure 4). It is therefore important to consider the increased risk that communities are in today compared to that in 1877 when assessing the effect of an 1877 size lahar in the future.

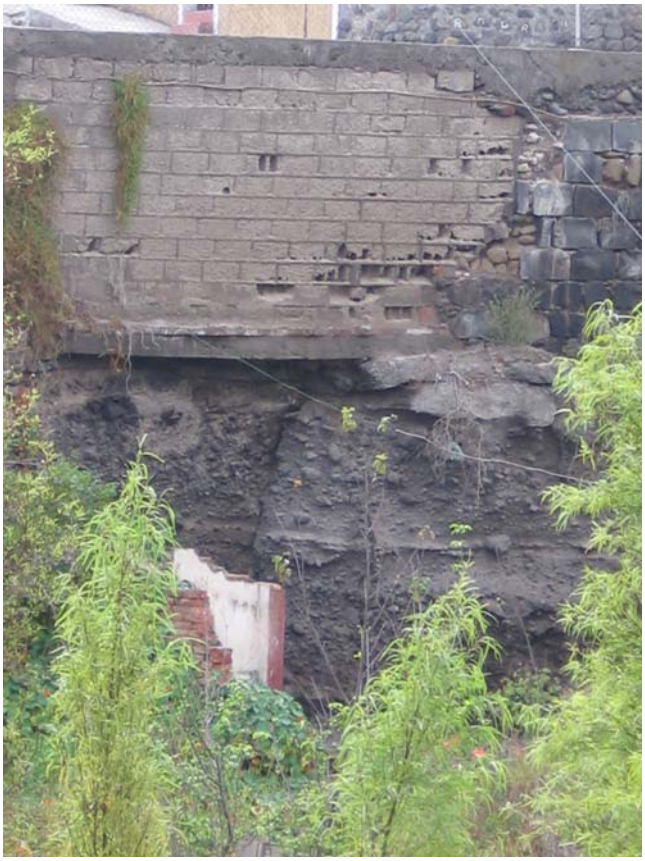

Figure 11: Buildings built upon 1877 (and older) lahar deposits.

Chapter 3 The 2005 Vazcún Valley Lahar: Evaluation of the TITAN2D Two-Phase Flow Model Using an Actual Event.

This chapter consists of a separate study to that carried out at Latacunga, Ecuador. This study presents an evaluation of the two-phase Titan2D model which incorporates the Pitman-Le two-phase debris flow model (Pitman and Le, 2005) into the existing Titan2D computational toolkit (Patra et al., 2005). An introduction to the model used in this study and for the Rio Cutuchi simulations is given. Comparisons are made between Titan2D simulations and recorded features of an actual event: The February 2005 Vazcún Valley Lahar. The Vazcún Valley drains from the northern slopes of Volcán Tungurahua, which lies approximately 80km south of Volcán Cotopaxi.

This location was chosen due to the small confined nature of the lahar. A detailed topographic survey, on the 1m scale, was attained in the field. This enabled a 5 m DEM to be derived (discussed later) which allowed for high resolution comparisons to be made. Other, well researched lahars may have large quantities of published data but lack the high resolution topographic data attainable at the Vazcún Valley. Detailed surveys, such as that undertaken in the Vazcún Valley so soon after the lahar, are not possible at other larger scale and better studied locations.

3.1 Two-Phase Titan2D

3.1.1 Pitman-Le Two-Phase Model

The Pitman-Le model is a depth averaged, thin layer model for geophysical mass flows which contain a mixture of solid material and fluid. It is derived from mass and

momentum balance laws based on a Coulomb constitutive description of dry granular material pioneered by Savage and Hutter (1989) and the 'two-phase' or 'two fluid' models commonly used in engineering. This hyperbolic system describes the motion of the two constituent phases and is fully explained in Pitman and Le (2005).

3.2.2 Titan2D toolkit

This mathematical model has been integrated into the existing Titan2D toolkit (Patra et al., 2005), which has previously been successfully used to simulate dry avalanches over realistic 3-D terrain (Sheridan et al., 2005). Titan2D utilizes adaptive grids, parallel processing and is integrated with the open-source GRASS Geographical Information System (GIS). Input parameters include initial pile volume, starting location, internal and bed friction angles, solid fraction and a base topography in the form of a Digital Elevation Model (DEM). It is able to produce simulations which output a variety of results including flow run-out, flow inundation area, velocity and flow depth, all of which can be animated.

3.3 The 2005 Vazcún Valley Lahar

3.3.1 Background

Located in the Eastern Cordillera, Volcán Tungurahua is one of Ecuador's most dangerous volcanoes. At 5023 m.a.s.l., Volcán Tungurahua towers above the surrounding landscape and in particular the city of Baños (pop. 18,000, el. 1800 m.a.s.l)(Figure 12). Since October 1999, Tungurahua has been in a state of near-continuous eruption characterized by small-moderate ash emission. Lahars have been a common occurrence

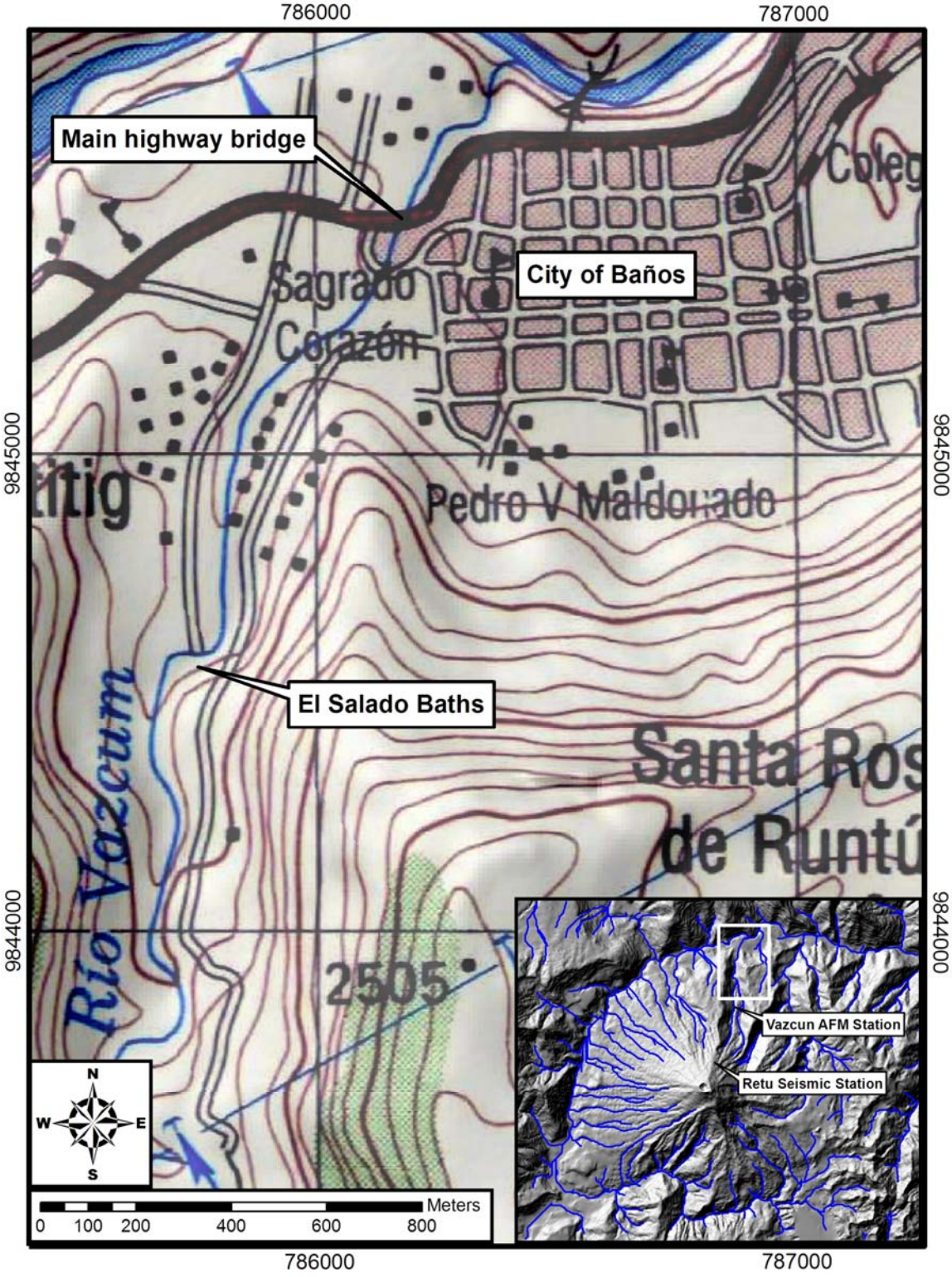

Figure 12: Map of the Vazcún Valley showing the location of important features mentioned in the text. Insert shows location of the Vazcún Valley on Volcán Tungurahua

.in several drainages around the volcano – 59 events between November 1999 and March 2002 (Sorenson *et al*., 2003). The flows have resulted in the temporary closure of the main Baños-Riobamba highway and nearly inundated the popular El Salado baths in the Vazcún Valley (Figures 12 and 14a). These lahars were caused by heavy rain remobilizing the ashfall deposits on the steep upper slopes of the volcano.

3.3.2 General description of the lahar

The following description is based on eyewitness accounts, video footage and written communications with scientists from Instituto Geofísico, Quito, and Civil Defense officials from the City of Baños. On February 12th, 2005, a lahar traveled the entire 10 km length of the Vazcún Valley. As with previous lahars at Tungurahua, this flow resulted from the remobilization of recent ashfall deposits by heavy rain. This was one of the largest events to have occurred in the Vazcún Valley since the current period of activity began in October 1999. The lahar was first recorded by the Retu seismic station (see location on Figure 12) at 17h59 local time. Approximately 13 minutes later, at 18h12, the lahar was first recorded on the Vazcún Acoustic Flow Monitor (AFM) and the instrument quickly became saturated. A further 16 minutes later, at 18h28, personnel from the Civil Defense reported the arrival of the first lahar wave at the El Salado baths, approximately 1 km outside of the city of Baños. The lahar continued in a series of pulses until approximately 19h10 when the last recognizable signal is seen on the AFM record. Based on the time of first detection by the seismic and AFM instruments, mean velocities for the lahar were calculated at 7 m s^{-1} for the stretch between the Retu seismic station and the Vazcún AFM, and 3.1 m s^{-1} for the section between the Vazcún AFM and the El

Salado baths. A volume of approximately 70,000 m^3 was estimated from the AFM records. After the event, scientists from Instituto Geofísico measured a series of cross-channel profiles in the vicinity of the EL Salado baths. Analysis of these profiles suggested a maximum flow rate of 100-104 $m^3 s^{-1}$, and a volume of 54,000 m^3.

Granulometry (Figure 13) of several samples of the deposit/veneer left behind shows that the majority (50-65%) of the lahar sediment comprised sand-size particles, a result of the source material being recent ashfall deposits. The samples also contained a large proportion of gravel-sized particles, many of which are rounded. This would suggest that the lahar has undergone a significant amount of bulking. Assuming that the gravel-sized particles represent the entrained material then the lahar has bulked by approximately 35%.

Although the 2005 Vazcún Valley Lahar is small when compared to lahars at other volcanoes (e.g., Nevado del Ruiz, 1985; Mt. Pinatubo, 1991-6; Mount St. Helens, 1980), it still presents a significant hazard to people and buildings located within or very close to the channel of the Río Vazcún. This particular flow came to within a few tens of centimeters of inundating the El Salado Baths, destroyed a small footbridge across the channel and piled several large boulders greater than 1 m in diameter against the base of the pier of the main highway bridge out of Baños (Figure 14).

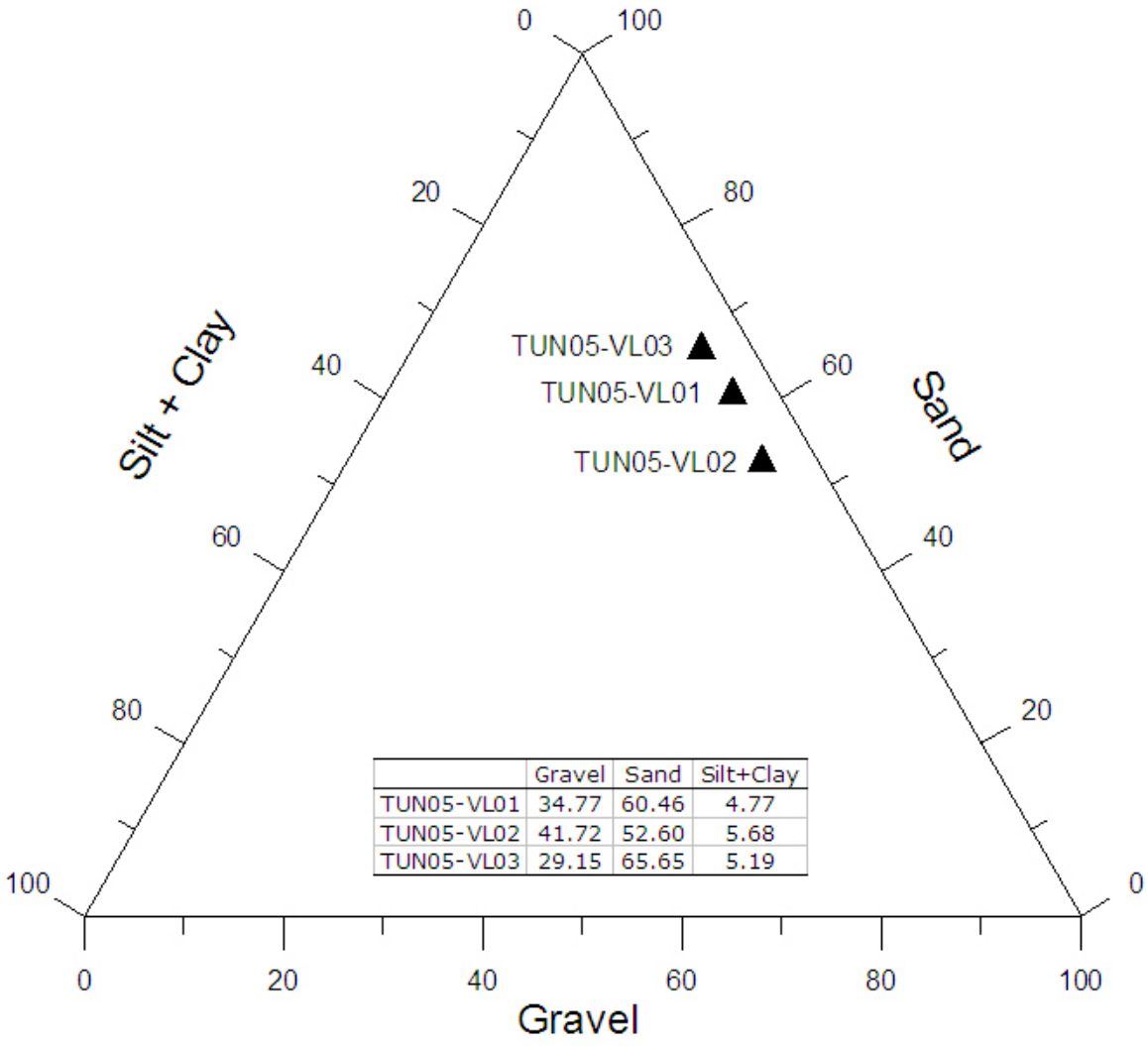

	Gravel	Sand	Silt+Clay
TUN05-VL01	34.77	60.46	4.77
TUN05-VL02	41.72	52.60	5.68
TUN05-VL03	29.15	65.65	5.19

Figure 13: Granulometry of the three lahar samples showing the relative proportions of gravel, sand and silt+clay.

3.4 Methods

3.4.1 Field Data Collection

In July 2005, five months after the event, evidence of the lahar (e.g. high flow marks) was still easily visible. As a result, a detailed survey of 1.6 km of the Vazcún Valley was completed using Differential GPS. More than 1500 data points with x, y, and z values

Figure 14: A) Photograph of the El Salado baths in the Vazcún Valley. At the weekends, it is estimated that more 300 people visit the baths per day. B) The 2005 Vazcún Valley Lahar came to within a few tens of centimeters of inundating the El Salado baths. Photograph shows lahar at peak stage height. Photograph courtesy of Defensa Civil de Baños. C) Looking downstream towards the new footbridge replacing the one destroyed by the lahar. Foreground shows area outside of channel inundated by the lahar. D) Meter-scale boulders piled up at the foot of the central support pier for the main road out of Baños. Note also splash/tide marks on both bridge piers.

were collected at intervals of approximately 5 m, with smaller spacing in areas of importance as identified in the field. Points were collected along the edges of the river

channel, along terraces and other breaks in slope, and also along the flow limit where visible.

3.4.2 Generation of Digital Elevation Model

The GPS survey data was processed and interpolated to create a digital elevation model (DEM) with 5x5 m cells. A pre-existing DEM with 10x10 m cells was created by Sorenson et al. (2003). This DEM was resampled to create 5x5 m cells and then merged with the newly created GPS-derived DEM. This was a necessary step because, despite having a 10x10 m cell size, the original source for the pre-existing DEM was a 1:50,000 scale topographic sheet with 40 m contour intervals. Consequently, the river channel and terraces are not well represented in the original 10 m DEM. Merging the two DEMs allows for potentially more accurate simulations.

3.4.3 Simulation Variables

Table 2 summarizes the range of input variables used in the simulations. The two end-member volumes are the two different values derived from the AFM records and the cross sections. Solid fractions cover the range of values that define debris flows (Sharp and Nobles, 1953; Pierson, 1980, 1985, Scott, 1988) as this parameter of the actual event is unknown, although considered to be on the higher end of the scale. Bed friction and internal friction angles were chosen based on previous work using Titan2D simulations. Sheridan et al. (2005) showed that simulations are not sensitive to internal friction angles so previously used angles are acceptable in this case. The simulations are, however, sensitive to bed friction angles but assessing this parameter is outside the scope of this

Parameter	Value
Volume m^3	50,000 and 70,000
Solid Fractions (0-1)	0.4, 0.5, 0.6, 0.7
Internal Friction Angle (°)	25
Bed Friction Angle (°)	10

Table 2: Summary of input parameters used in simulations.research

and is an ongoing project. The bed friction angle used is within the range of values often used for glacial and fluvial deposits (Stinton et al., 2004).

3.5 Results

Figures 15-19 show results generated by the Titan2D simulations for the February 2005 Vazcún Valley Lahar. A summary of these results are shown in Table 3.

	Field Data	Simulation output
Velocity: Upper Channel (ms^{-1})	7	5.8-8.9
Velocity: Lower Channel (ms^{-1})	3.1	1.1-2.6
Flow Thickness (m)	2.8	2.9
Run Up Height (m)	5.5	6.7

Table 3: Summary of results.

3.6 Discussion

The performance of the Titan2D model in simulating the 2005 Vazcún Valley Lahar was evaluated by considering a variety of properties, each discussed here. Comparisons were made between model outputs and field-recorded inundation areas, velocities, flow thicknesses and run up heights.

3.6.1 Flow simulations and Inundation Areas.

Flows were simulated using a variety of solid fraction ratios and the two end-member volume estimates (50,000 m^3 and 70,000m^3). Figure 15 shows the final time steps for two simulations of 70,000m^3 with different solid fractions of 40% (Figure 15a) and 60% (Figure 15b). The 60% solid fraction flow behavior was closest to that of the actual flow, and is used for the pile height and run-up height comparisons. The AFM-calculated volume of 70,000 m^3 is considered the more reliable estimate and it behaved closest to the actual flow in the simulation and is therefore used in the later comparisons rather than the 50,000 m^3 volume. Both flows were predictably constrained to the channel and produced inundation areas that match the inundation areas mapped in the field.

3.6.2 Velocity

The Titan2D model predicted velocities that are within 17-27% of the recorded velocity in the upper part of the channel. Velocities in the lower part of the channel were underestimated but were accurate to within 17-67% of the velocities recorded for this section. It should be noted that errors in the recorded velocities have not been determined.

Velocities are commonly used in model evaluations but comparisons of such simulations are difficult. The average velocities recorded here are computed by considering the velocity of various computational cells which range from 0 ms^{-1} to values way above the mean. Average velocities from simulations are reported for simplicity. It is therefore clear that these values will not be the same as velocities seen when watching the flow or recorded by devices that record the arrival of the flow front.

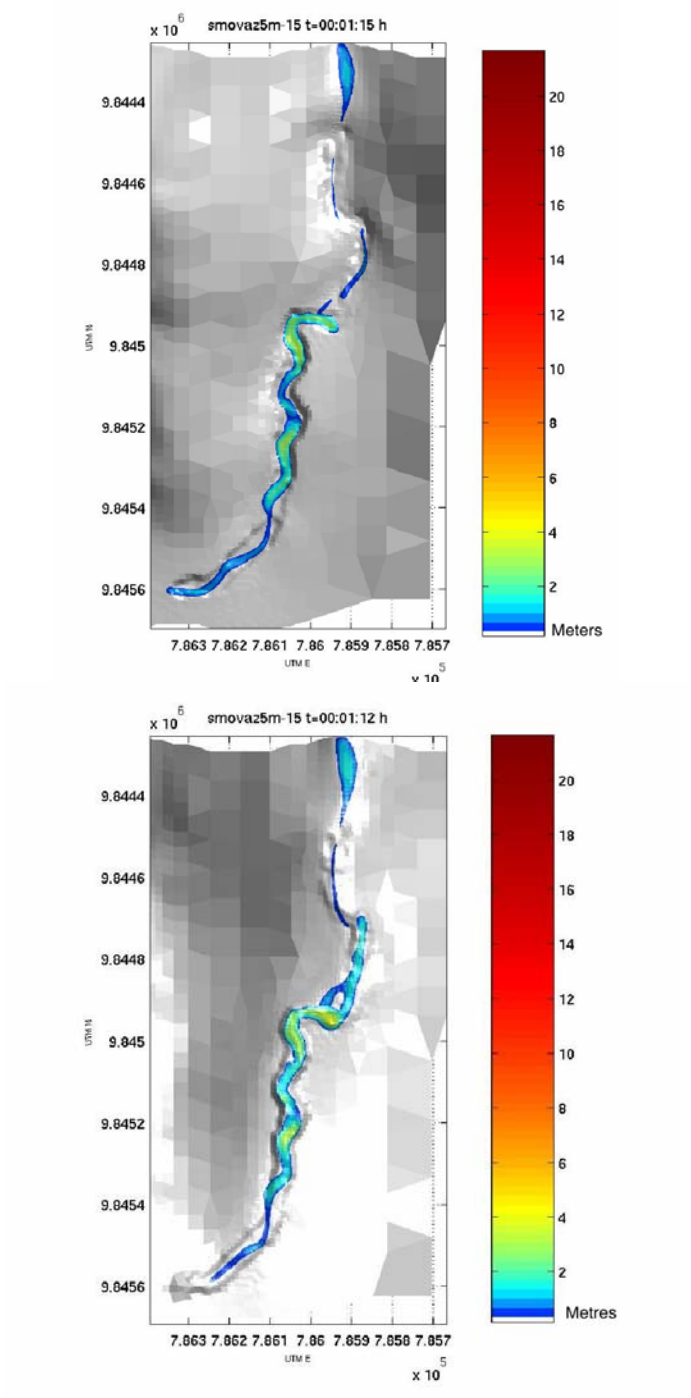

Figure 15: Final timesteps for simulations of 70,000 m^3 for a) 40% solid fraction and b) 60% solid fraction. Note the confinement of the flow to within the channel.

3.6.3 Flow Thickness

Flow thickness at measured at El Salado baths were compared with Titan2D calculated flow thickness in the same section of the channel (Figure 17). Titan2D overestimated flow thickness in this section by 0.11 m, which is within 4% of the measured flow thickness. Flow thickness is a good parameter for comparisons as no averaging is required and it is not highly dependent on boundary conditions.

3.6.4 Run-up Heights

Titan2D simulations display super-elevation around bends in the channel the same way an actual flow does. Figure 18 shows profiles across the simulated flow and the actual flow in a section of the channel that has undergone superelevation. Field cross sections show superelevation of 5.5 m and the Titan2D simulations produced a run-up height of 6.65 m. The simulated flow had a run-up within 21% of the actual flow.

3.7 Conclusions

The purpose of this study was to evaluate the performance of the two-phase Titan2D flow model in simulating an actual event whose flow features were observed and studied in detail. The simulations yielded by the two-phase Titan2D are in close agreement with the behavior of the 2005 Vazcún Valley Lahar. The model was able to effectively simulate flow depth, run-up heights, inundation area and to some extent, the average velocity of the flow.

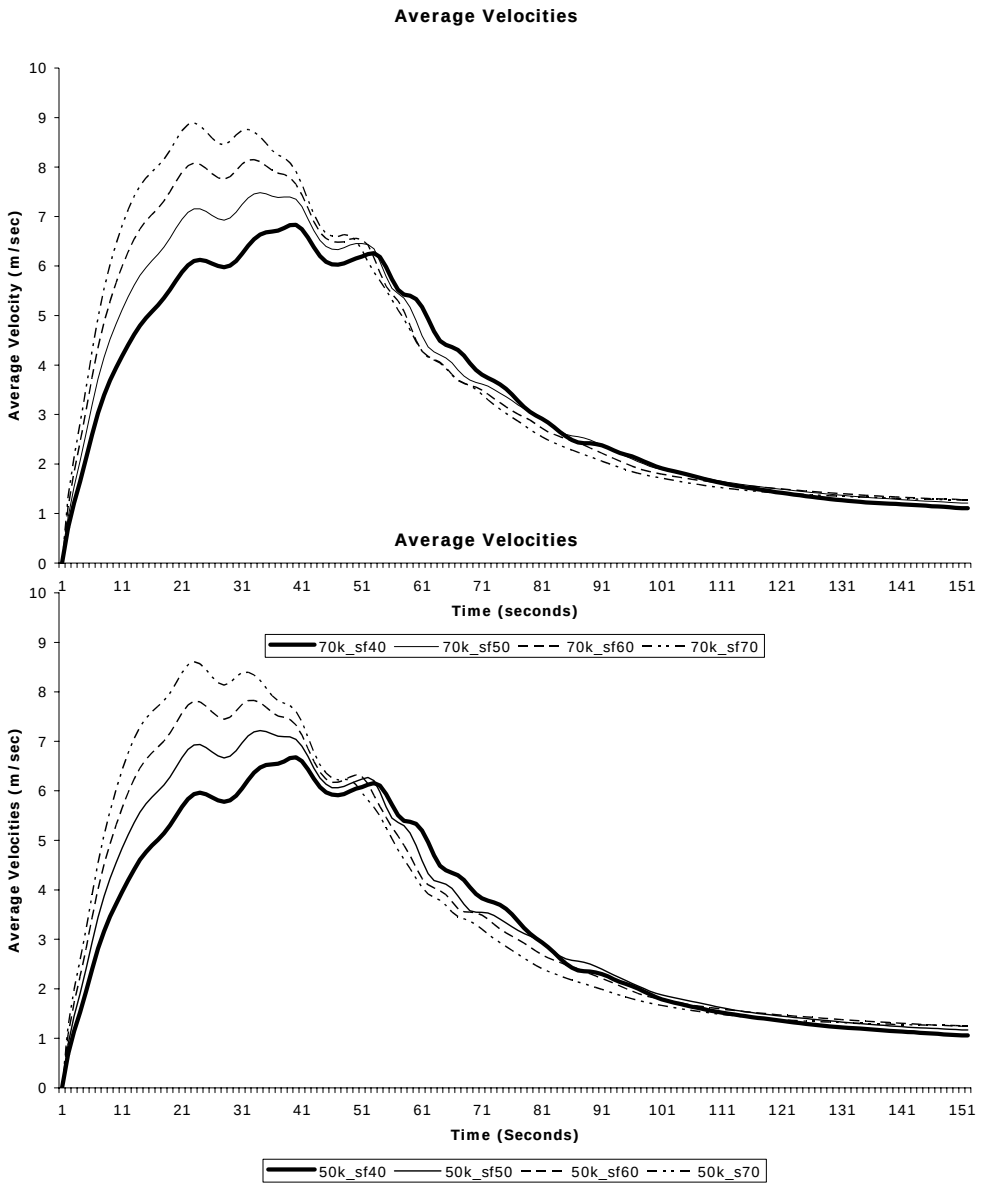

Figure 16: Velocity vs time plots for a) 70,000 m^3 (70k) simulations and b) 50,000 m^3 (50k) each for 40 (sf40), 50 (sf50), 60 (sf60) and 70% (sf70) solid fractions. Velocities at the start of the simulations (in the upper parts of the channel) reach velocities of 6-9 ms^{-1}, with velocities towards the end of the simulations (lower parts of the channel) have constant velocities of 1-3 ms^{-1}.

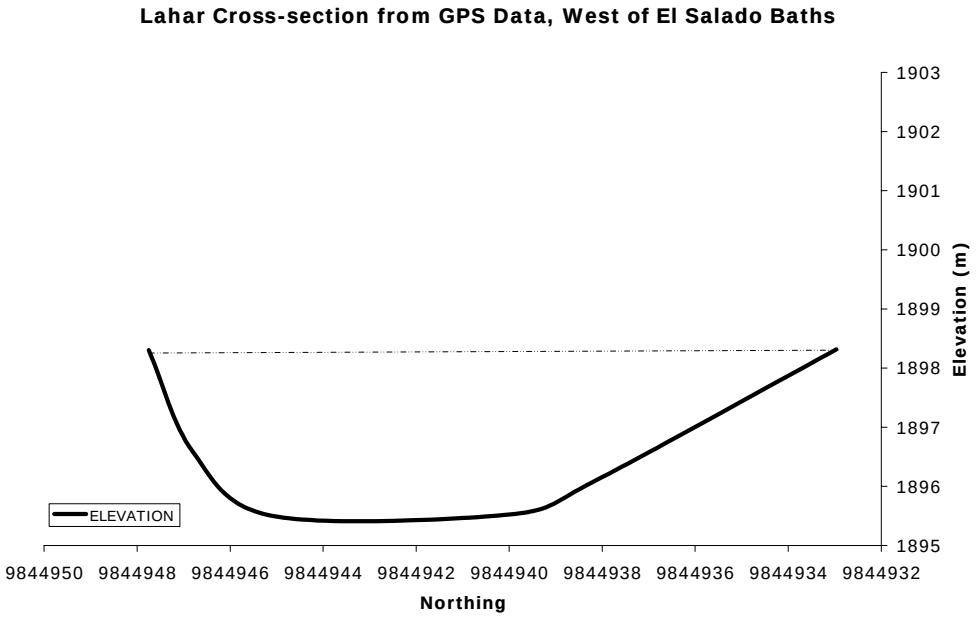

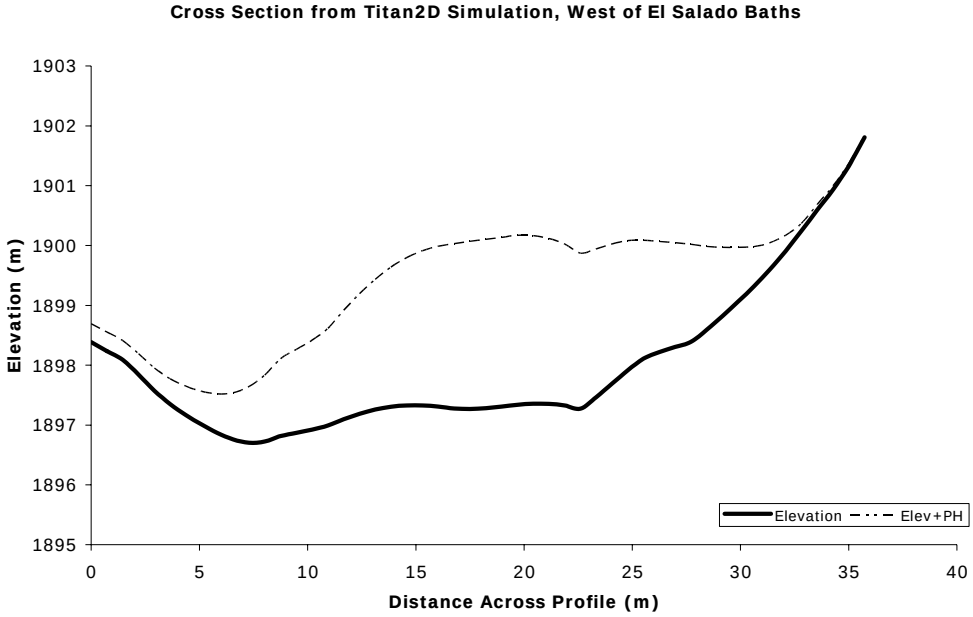

Figure 17: Cross section taken at the El Salado Baths from a) GPS data and b) Titan2D simulation. Solid line indicates underlying topography, the dashed line indicates maximum flow height. Flow edges seen in the GPS profile are actual flow extents measured in the field.

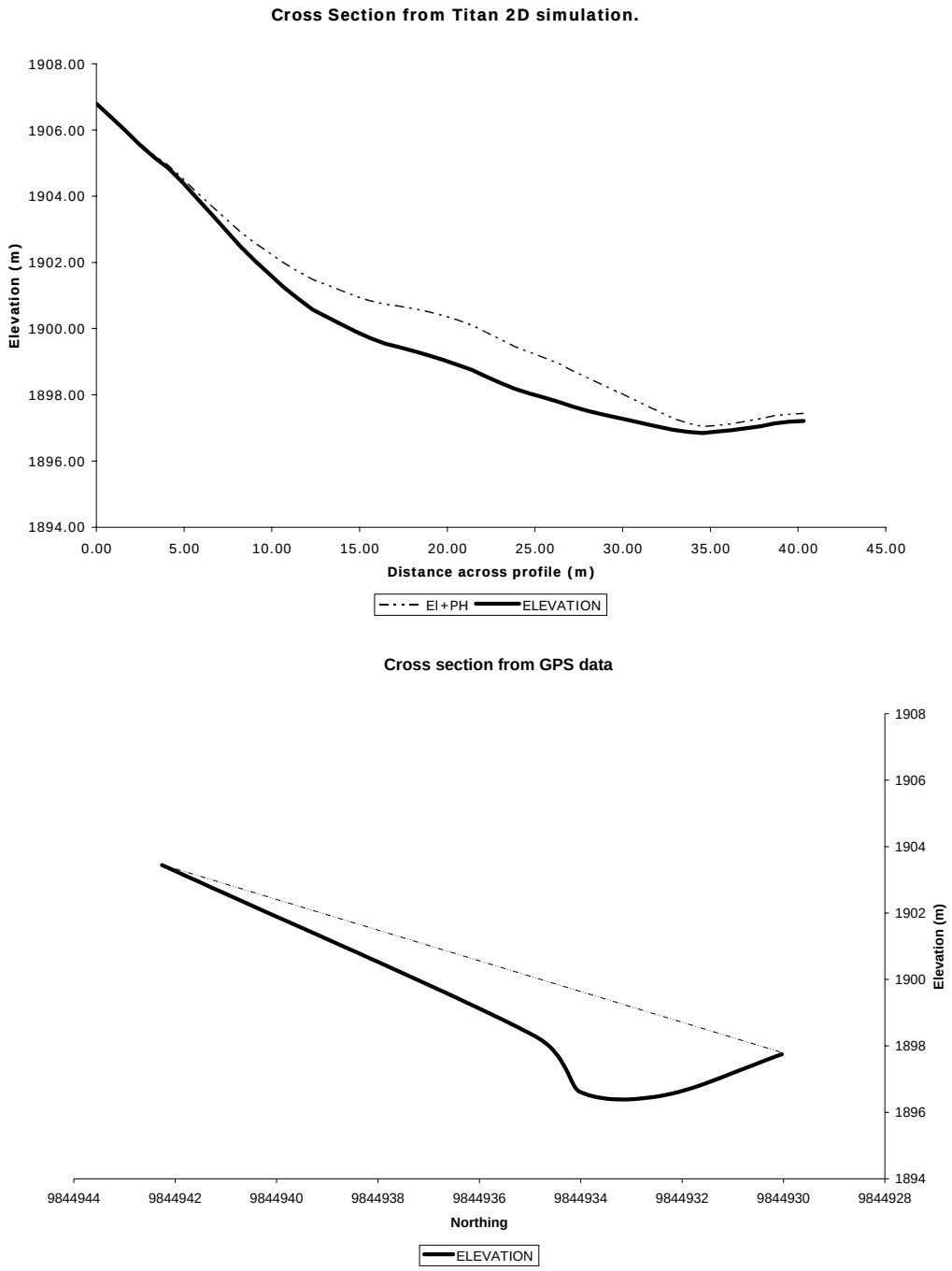

Figure 18: Cross sections of a section of the channel that experienced superelevation from a) the GPS data and b) the Titan2D simulation. Again, solid lines represents underlying topography and the dashed line represents maximum flow height. Flow edges in the GPS profile are actual flow extents measured in the field.

Chapter 4 Simulating Potential Lahars using Titan2D for the Río Cutuchi

Previous works on simulating lahars for Volcán Cotopaxi have concentrated on recreating the 1877 event (Barberi et al., 1992; Aguilera et al., 2004). The aim of this study is to consider a variety of 'what if' scenarios and does not attempt to constrain its hazard analysis to one size event. With this in mind, a modeling technique that could easily be applied to a variety of volumes was needed.

Titan2D is a thin-layer, depth-averaged geophysical mass flow model that has previously been used to model dry avalanches and pyroclastic flows (Patra et al., 2005). A new development, the two-phase model based on the two-fluid Pitman Le model (2005) is now available for use on debris flows. This model has been evaluated using an actual event, the February 2005 Vazcún Valley Lahar (as described in Chapter 3) and was considered the best model available for this study.

Titan2D has several advantages over other models that are in existence such as FLO-2D (O'Brian et al., 1992), LaharZ (Iverson et al., 1998) and DAMBRK (Fread 1988, Costa 1997) in that it was designed specifically with debris flows in mind (FLO-2D and DAMBRK are primarily stream flow models) and is based on geophysical laws.

Currently, the most widely used application for lahar hazard assessment is LaharZ. The basis of this model is the application of two scaling relationships that relate the volume of

the lahar to the cross-sectional area and planimetric area. The output is inundation area and flow depth. The Titan2D model is based on first principles of physics (Iverson, 1997; Savage and Hutter, 1989) rather than statistical relationships. The model outputs include travel time and velocity (momentum), flow thickness and inundation areas. This aids in improvements in warning systems as expected inundation times can be derived.

The Titan2D model requires several user-defined input parameters including 3D topography, volumes, solid fraction, internal friction angle and bed friction angle.

4.1 Topographic Data

Titan2D requires topographic data in the form of a digital elevation model (DEM) stored in the Geographic Information System (GIS) freeware, GRASS (http://grass.itc.it). This study utilizes a DEM acquired by the Shuttle Radar Topography Mission (SRTM). This dataset is freely available from the SRTM website as a 90 meter grid. Whilst this is somewhat of a coarse resolution, the DEM is correct for the study area: the stream network derived from this DEM matches the actual stream network, mainly the Rio Cutuchi. SRTM data has been analyzed for height error and the results are summarized in Table 4. Confidence is placed in this DEM over other datasets available. These other datasets are 30 meter and 50 meter DEMs which have been digitized from topographic maps at the 1:50,000 scale. These DEMs are not correct for the city of Latacunga as they do not place the Rio Cutuchi in the right place when the stream network is derived, and contain many artifacts that are related to the topographic maps and the digitizing process.

	Africa	Australia	Eurasia	Islands	N. America	S. America
Absolute Geolocation Error	11.9	7.2	8.8	9.0	12.6	9.0
Absolute Height Error	5.6	6.0	6.2	8.0	9.0	6.2
Relative Height Error	9.8	4.7	8.7	6.2	7.0	5.5
Long Wavelength Height Error	3.1	6.0	2.6	3.7	4.0	4.9

Table 4: Summary of SRTM height performance. All quantities represent 90% errors in meters (Rodriguez et al., 2005)

4.2 Simulation Variables.

Table 5 summarizes the range of input variables used in the simulations, which are discussed in detail in the following section. The simulated flows were all initiated in the same location in the Rio Cutuchi several kilometers above the city of Latacunga. This allows a detailed look at the effect of flows on the city without the consumption of large amounts of computational time. Starting flows at the source is not possible at this time

Run	Volume m^3	Solid Fractions	Internal Friction Angle (°)	Bed Friction Angle (°)
1a	10×10^4	0.65	25	10
2a	60×10^4	0.65	25	10
3a	10×10^5	0.65	25	10
4a	60×10^5	0.65	25	10
4b	60×10^5	0.70	25	10
4c	60×10^5	0.75	25	10
4d	60×10^5	0.65	25	14
4e	60×10^5	0.65	25	17
5a	10×10^6	0.65	25	10
6a	60×10^6	0.65	25	10
6b	60×10^6	0.70	25	10
6c	60×10^6	0.75	25	10
6d	60×10^6	0.65	25	14
6e	60×10^6	0.65	25	17
7a	10×10^7	0.65	25	10

Table 5: Summary of input parameters for all runs. Note that some volumes have varied solid fractions and bed frictions so that the effect of these parameters could be investigated.

due to the very long wall-time involved in these simulations. Flows were started upstream of the city to ensure the flow had stabilized before reaching Latacunga so that original pile shape would have no effect on inundation area.

4.2.1 Volumes

The aim of this study was to consider a range of 'what if' scenarios and not to attempt to recreate any particular historic flow. A starting volume of 60 x 10^6 m^3 was based on volumes previously estimated for the 1877 lahar (Barberi et al., 1991; Mothes, 2006). To ensure a range of volumes that will cover all possible events, two volume values for each order of magnitude were used ranging from 10^4 to 10^7 m^3.

4.2.2 Solid Fraction

Solid fractions for debris flows are considered to have in excess of 60% solid fraction (by volume) and 80% by weight (Costa, 1984, 1988; Pierson and Costa, 1987). The initial solid fraction value used (0.65) in the simulations is the median value for the volume proportions typical of debris flows (Sharp and Nobles, 1953; Pierson, 1980, 1985, Scott, 1988). To consider the solid fraction used in previous studies (Barberi et al., 1992) and to account for the full range of possible fractions, certain simulations used 0.7 and 0.75 solid fraction by volume.

4.2.3 Internal Friction Angle

The internal friction angle was chosen to be consistent with the successful 2005 Vazcún Valley Lahar simulations, described in Chapter 3

4.2.4 Bed Friction Angle

The initial bed friction angle (10°) was the same as that used for the 2005 Vazcún Valley simulations. This angle is used for the majority of the simulations; however, the effect of different bed friction angles was also tested for the Rio Cutuchi. Two other values were chosen for the bed friction angle so that the range of angles (9°-17°) for fluvial deposits (Stinton et al., 2004) could be considered.

4.3 Results

Successful simulation outputs were obtained for runs 2a through 8a. Due to the early developmental stage of the two-phase model, initiating a flow that would travel the Latacunga Valley was difficult. Problems were faced with pile shape and height, DEM size, number of computational mesh points, memory crash and extremely long computational time. Here, successful runs are defined as simulations for which an output was achieved. The simulations output grass sites files (for use in the GIS GRASS) and a text file readable in excel. Results are reported here as an inundation map (Figure 19). This map shows the discrete point-data sets imported from the GRASS .sites files overlayed on a topographic map for the area. This map was compiled within ArcGIS, which required some conversion of the data from the original grass sites files, but no information was lost in the process. It shows that volumes of less than 6 million m^3 are mostly contained with the channel and do not inundate large areas of the city. Larger volumes overbank the channel in Latacunga. The volume in run 1a was too small to be effectively simulated by the Titan2D model and is therefore not reported here.

The simulations show that a lahar passing through Latacunga would likely have a low average velocity of <1 ms^{-1} to 2 ms^{-1} (refer to Chapter 3 on why average velocity should be considered with caution) and with a low flow height of <1 m to 3 m. This is most likely due to the low-gradient and broad width of the valley at this location.

4.3.1 Effect of solid fraction.

Solid fraction was considered for two different volumes (60 x 10^5 m^3 and 60 x 10^6 m^3) with all other variable held constant. Figure 20 shows the inundation areas produced for the range of solid fractions for both volumes. Whilst there is some change on the cell-scale, there is little overall effect on inundation area when solid fraction is changed.

4.3.2 Effect of bed friction.

The same two volumes were also used to consider the effect of bed friction. The model is known to be sensitive to bed friction and therefore a suitable value must be considered carefully for successful simulations.

Figure 21 shows the effect of bed friction on inundation area for both volumes. The smaller volume shows an increase in inundation area with increasing bed friction. However, the larger volume shows little change of inundation area with changing friction values.

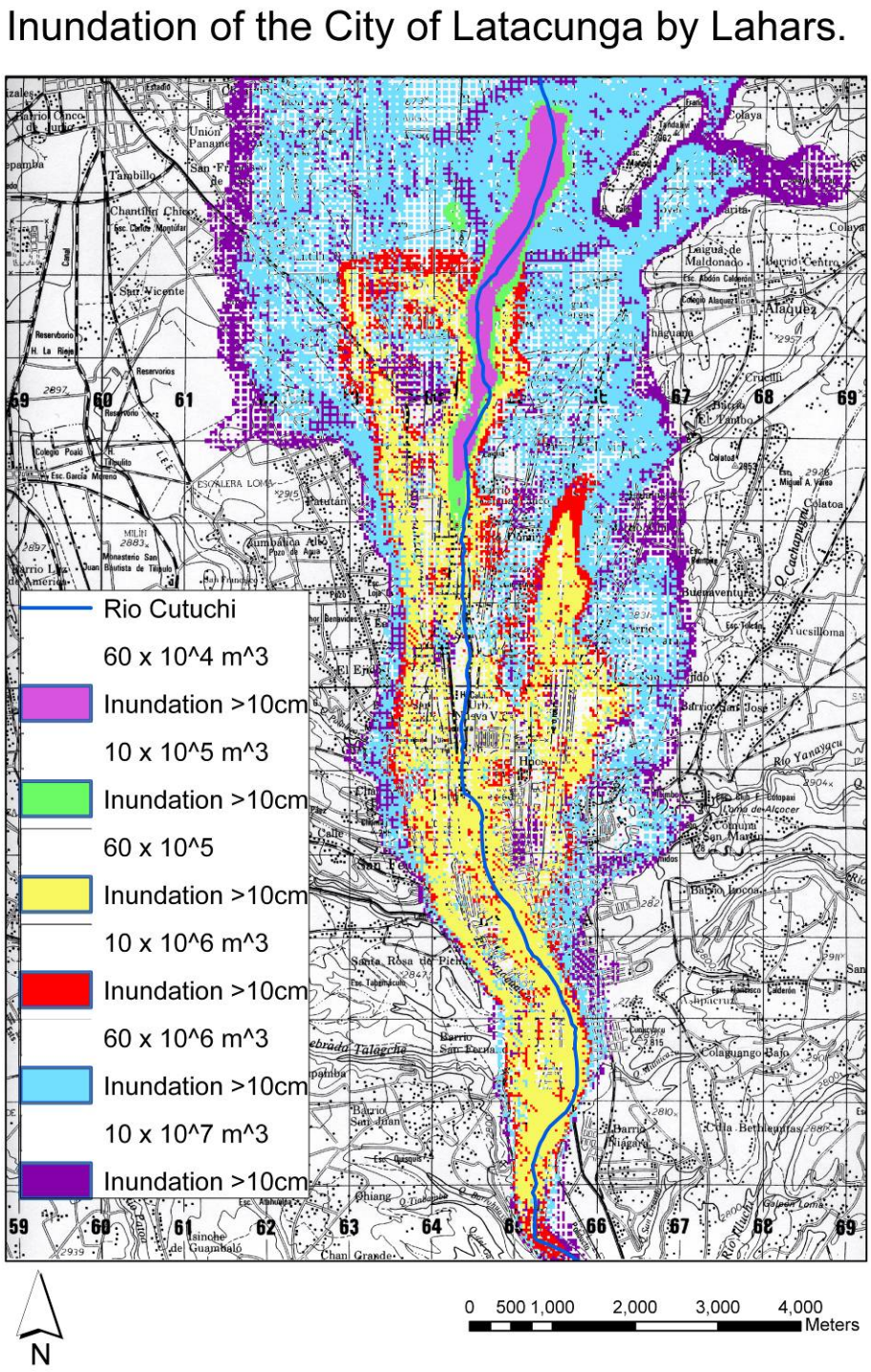

Figure 19: Preliminary inundation map for the Latacunga Valley for various scale lahars.

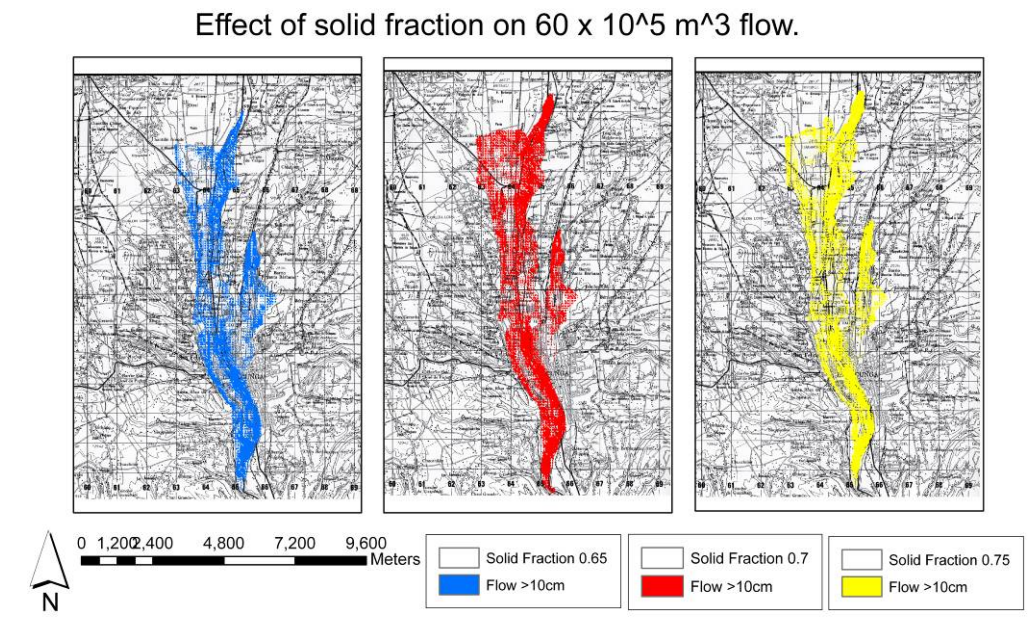

a)

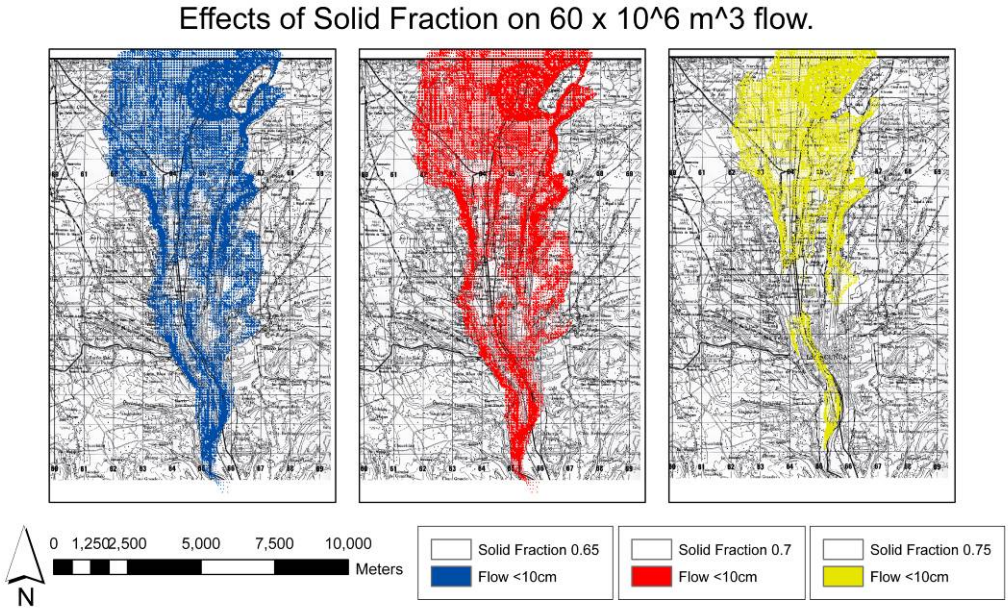

b)

Figure 20: Investigating the effects on inundation by varying solid fraction for a) 60 x 10^5 m^3 and b) 60 x 10^6 m^3. Note that there is very little change in overall area of the flow. For the higher solid fraction, slightly more of the flow appears the be constrained to the Rio Cutuchi, this however, does not greatly impact the overall flow inundation area.

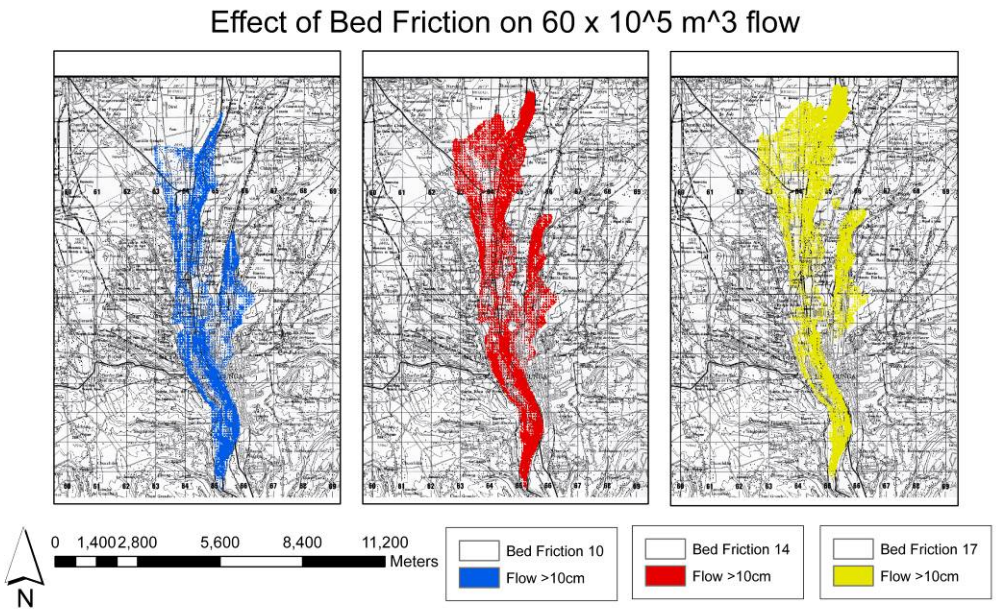

a)

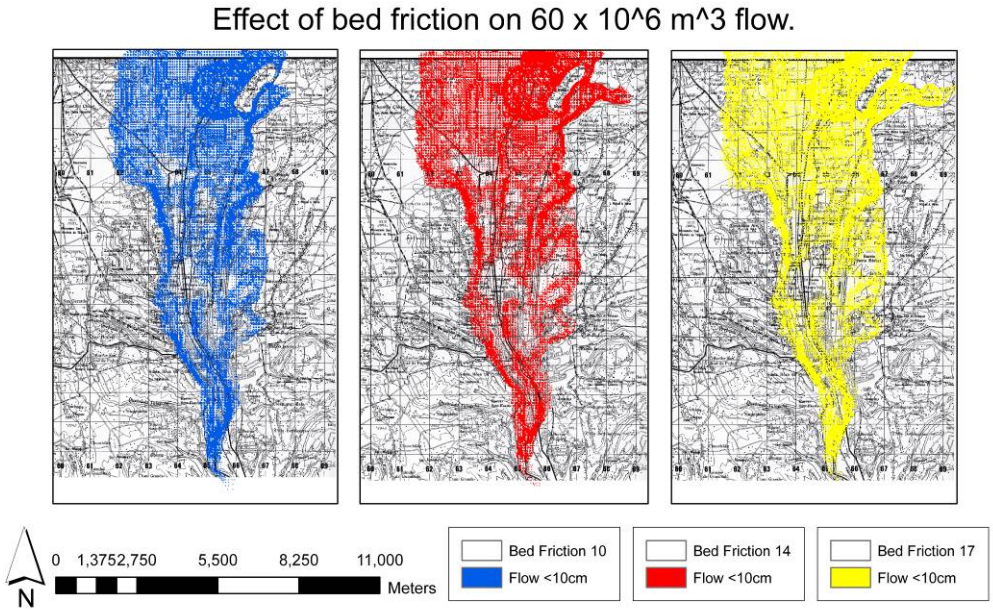

b)

Figure 21: Investigating the effect on inundation by varying Bed friction for a) 60 x 10^5 m^3 and b) 60 x 10^6 m^3. Similarly to the solid fraction, changing bed friction has very little effect on the general inundation area.

Chapter 5 Map of Probabilistic Lahar Inundation for the City of Latacunga

5.1 Introduction

This study uses a two-step approach in assessing the impact on Latacunga by various scale lahars in the event of a future eruption of Volcán Cotopaxi. Firstly, inundation maps produced using simulations in Titan2D are used to generate probabilistic inundation maps for the city. This considers not only the probability of a certain size lahar inundating a particular area, but also the probability of such a size lahar occurring. The second step is to make a detailed analysis of the city with regards to the location of hospitals, population centers, schools, major roadways and bridges etc. Combining this analysis with probabilistic inundation will allow vulnerability to be realistically quantified.

5.2 Probabilistic Inundation Map

The probability of a particular size lahar occurring is key to understanding the likelihood of inundation for the city of Latacunga. This probability was derived from linking a certain size lahar to a Volcanic Explosivity Index (VEI) value based on eruption scenarios and historical data and then calculating the eruption frequency for each VEI. Therefore, using a simple probability function (Equation 2) the conditional probability of inundation by lahar was calculated.

$$P_c = (P_i \mid P_e) \qquad (2)$$

Where P_c is the conditional probability of inundation by lahar, P_i is the probability of inundation by a flow thicker than 10 cm (0 or 100%) and P_e is the probability of a particular size eruption occurring based on eruptive frequency (0 to 100%). The logic tree illustrated in figure 22.

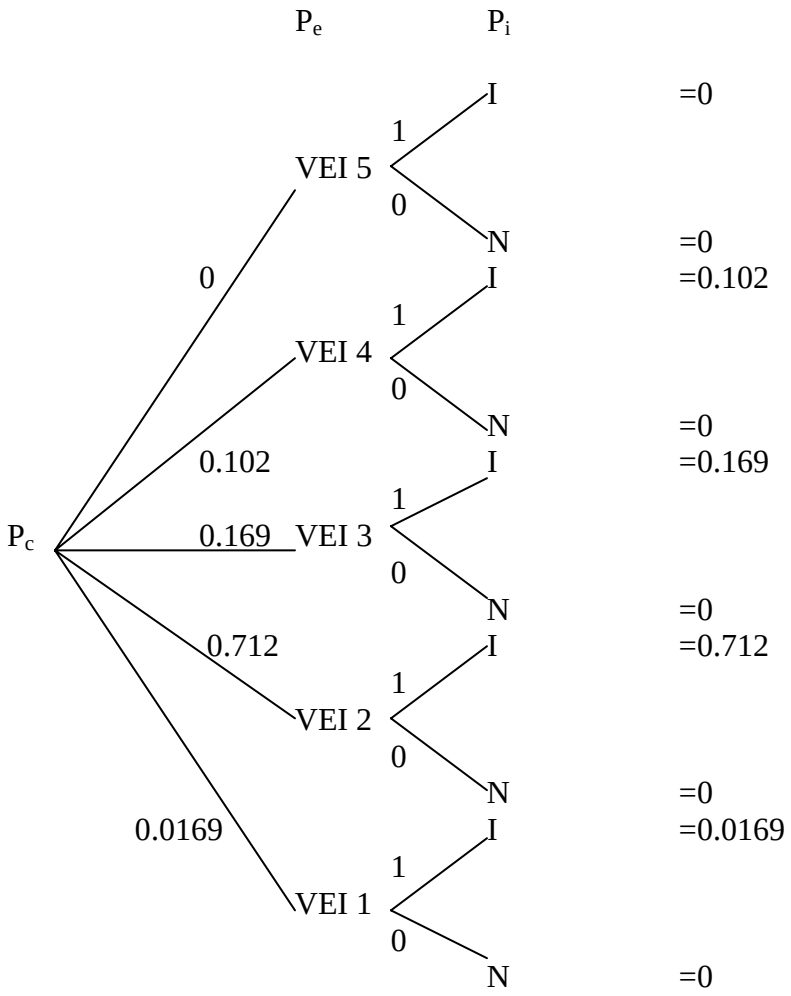

Figure 22: Probability Tree. Where P_c is the conditional probability for inundation, P_e is the discrete probability of eruption, and P_i is the binary probability of an individual cell being inundated (I = inundated, N = no inundation). Pe is based on historical data for Cotopaxi and is discussed later in this chapter.

5.2.1 Eruptive Scenarios and Historical Data as a guide to linking particular lahar volumes to VEI values.

Andrade et al., (2005) considered four likely eruptions scenarios for Volcán Cotopaxi which are based on a series of VEI-sized eruptions. The first considers a small event (VEI 1-2) which is typified by Strombolian activity. This type of activity would likely become the 'background' activity in the event of the initiation of activity at Volcán Cotopaxi. It is predicted that scenario 1 would involve small-moderate ash emissions and small lava flows. This may result in the generation of small to moderate size primary or secondary lahars that would not reach the inhabited areas of the province.

Scenario 2 takes into account a moderate event (VEI 2-3) characterized by violent Strombolian to Vulcanian activity. This scenario considers locally important ash emissions, pyroclastic flows and lava flows of little extension. Historic eruptions fitting this scenario include the 1853-1854 eruptive period which caused moderate sized lahars that represent a direct threat to the population along the main drainages of the volcano.

The third scenario considers a great event (VEI 4) similar to that of the 1877 eruption. Activity would be Vulcanian to Sub-Plinian with ash emissions that would affect distal communities. Pyroclastic flows (most likely of a 'boiling-over' nature) are likely to occur, which would simultaneously descend several or all flanks of the volcano. Lahars of great volume are expected to occur as a result of the interaction between the pyroclastic flows and the summit glaciers. These lahars would cause devastation along the main drainages of the volcano and may take hundreds of kilometers to dilute to

hyperconcentrated stream flow. Andesitic lava flows are predicted in the crater but would not extend below 3500 m. This scenario occurred frequently in the past, particularly in the years 1742, 1744, 1768 and 1877.

Scenario 4 is a very large event of VEI 4-5 and corresponds to a Plinian eruption. This highly explosive activity would result in ash accumulation of 1 -1.5 meters up to 10 km from the summit. The column would collapse to form pyroclastic flows that could reach up to 20-25 km from the crater. Consequent lahars would be greater than any recorded in historical times and would approach the size of the Chillos Valley Lahar.

A simple table is reported here (Table 6, part II) as a guide to the link between eruptive size and lahar size. This data, and published volumes for the 1877 and CVL lahars (Mothes, 1991; Barberi et al, 1992; Mothes et al., 1998; Aguilera et al., 2004) are combined with the eruption scenarios outlined by Andrade et al., (2005) to associate a VEI to the range of lahar volumes used in the simulations (Table 7).

5.2.2 Eruption Frequency

Eruption frequency for each value of VEI (1-5) was calculated for all historical eruptions (since 1532) based on data presented by Siebert and Simkin (2002), summarized in Table 6 part I. These eruption frequencies are presented in Table 7 for each VEI. It is important to note that eruption frequency data differs depending on the source (Siebert and Simkin, 2002; Barberi et al., 1992; Mothes 1991, 2006) and therefore the probability of occurrence is likely to differ depending on which source is used. Siebert and Simkin

Part I

Siebert L, Simkin T (2002-)

Start: Year	Start: MoDy	Stop: Year	Stop: MoDy	Place of Eruption	Tephra	Lava	Damage	VEI
1942	217	1942	219	Central crater eruption	Explosive	- - - -	Damage (Land, property, etc)	3?
1940	. . . .	. . . .	. . . .	Central crater eruption	Explosive	- - - -	- - - -	2
1939	202	. . . .	. . . .	Central crater eruption	Explosive	- - - -	- - - -	2
1931	. . . .	. . . .	. . . .	Central crater eruption	Explosive	- - - -	- - - -	2
1926	. . . .	. . . .	. . . .	Central crater eruption	Explosive	- - - -	- - - -	2
1922	. . . .	. . . .	. . . .	Central crater eruption	Explosive	- - - -	- - - -	2
1908	. . . .	1914	. . . .	Central crater eruption	Explosive	- - - -	- - - -	1
1907	06 . .	. . . .	. . . .	Central crater eruption	Explosive	- - - -	- - - -	2
1906	821	1906	919	Central crater eruption	Explosive	- - - -	- - - -	2
1905	. . . .	. . . .	. . . .	Central crater eruption	Explosive	- - - -	- - - -	2
1903	926	1904	12 . .	Central crater eruption	Explosive + Pyroclastic Flows	- - - -	Lahars	3
1895	. . . .	. . . .	. . . .	Central crater eruption	Explosive	- - - -	- - - -	2
1886	01 . .	. . . .	. . . .	Central crater eruption	Explosive	- - - -	- - - -	2
1885	723	. . . .	. . . .	Central crater eruption	Explosive + Pyroclastic Flows	- - - -	Lahars	2
1883	12 . .	. . . .	. . . .	Central crater eruption	Explosive + Pyroclastic Flows	- - - -	Lahars	2
1883	08 . .	. . . .	. . . .	Central crater eruption	Explosive + Pyroclastic Flows	- - - -	Lahars	2
1882	01 . .	1882	03 . .	Central crater eruption	Explosive	- - - -	- - - -	2
1880	02 . .	1880	07 . .	Central crater eruption	Explosive + Pyroclastic Flows	- - - -	Lahars	3
1879	226	1879	619	Central crater eruption	Explosive + Pyroclastic Flows?	- - - -	- - - -	2
1878	823	1878	824	Central crater eruption	Explosive + Pyroclastic Flows	- - - -	- - - -	2
1877	01 . .	1877	902	Central crater eruption	Explosive + Pyroclastic Flows	- - - -	Fatalities, Damage, Lahars	4
1870	. . . .	1876	. . . .	Central crater eruption	Explosive	- - - -	- - - -	2
1869	07 . .	1869	08 . .	Central crater eruption	Explosive	- - - -	- - - -	3

1868	815	1868	816	Central crater eruption	Explosive	- - - -	- - - -	2
1867	. . . .	. . . .	. . . .	Central crater eruption	Explosive	- - - -	- - - -	2
1866	921	1866	926	Central crater eruption	Explosive	- - - -	- - - -	2
1863	. . . .	. . . .	. . . .	Central crater eruption	Explosive + Pyroclastic Flows	- - - -	Lahars	2
1860	. . . .	1862	. . . .	Central crater eruption	Explosive	- - - -	- - - -	2
1859	. . . .	. . . .	. . . .	Central crater eruption	Explosive	- - - -	- - - -	2
1858	11 . .	1858	12 . .	Central crater eruption	Explosive + Pyroclastic Flows	- - - -	Lahars	2
1857	. . . .	. . . .	. . . .	Central crater eruption	Explosive	- - - -	- - - -	2
1856	10 . .	1856	12 . .	Central crater eruption	Explosive + Pyroclastic Flows	- - - -	Lahars	2
1856	05 . .	. . . .	. . . .	Central crater eruption	Explosive + Pyroclastic Flows	- - - -	Lahars	2
1855	11 . .	. . . .	. . . .	Central crater eruption	Explosive + Pyroclastic Flows	- - - -	Lahars	2
1854	914	. . . .	. . . .	Central crater eruption	Explosive + Pyroclastic Flows	- - - -	Lahars	2
1854	403	. . . .	. . . .	Central crater eruption	Explosive + Pyroclastic Flows	- - - -	Lahars	2
1853	913	1853	915	Central crater eruption	Explosive + Pyroclastic Flows	Lava Flows	Lahars	3
1852	. . . .	. . . .	. . . .	Central crater eruption	Explosive	- - - -	- - - -	2
1851	06 . .	. . . .	. . . .	Central crater eruption	Explosive	- - - -	- - - -	2
1850	. . . .	. . . .	. . . .	Central crater eruption	Explosive + Pyroclastic Flows	- - - -	Lahars	2
1845	04 . .	. . . .	. . . .	Central crater eruption	Explosive	- - - -	- - - -	2
1844	. . . .	. . . .	. . . .	Central crater eruption	Explosive	- - - -	- - - -	2
1803	104	1803	105	Central crater eruption	Explosive + Pyroclastic Flows	- - - -	Damage, Lahars	3
1768	404	. . . .	. . . .	Central crater eruption	Explosive + Pyroclastic Flows	- - - -	Fatalities, Damage, Lahars	4
1766	210	1766	12 . .	Central crater eruption	Explosive + Pyroclastic Flows	- - - -	Damage, Lahars	3
1750	0902a	1750	0904a	Central crater eruption	Explosive	- - - -	- - - -	2
1747	. . . .	1749	. . . .	Central crater eruption	Explosive	- - - -	- - - -	2
1746	02 . .	. . . .	. . . .	Central crater eruption	Explosive	- - - -	- - - -	2
1744	05 . .	1744	12 . .	Central crater eruption	Explosive + Pyroclastic Flows	Lava Flows?	Damage, Lahars	4
1743	927	1743	1004	Central crater eruption	Explosive + Pyroclastic Flows	- - - -	Lahars	2

1743	04 . .	. . . .	. . . .	Central crater eruption	Explosive + Pyroclastic Flows	- - - -	Damage, Lahars	4
1742	1209	. . . .	. . . .	Central crater eruption + Radial Fissure Eruption	Explosive + Pyroclastic Flows	- - - -	Fatalities, Damage, Lahars	3?
1742	615	1742	07 . .	Central crater eruption	Explosive + Pyroclastic Flows	- - - -	Fatalities, Damage, Lahars	4
1740	. . . .	1741	. . . .	Central crater eruption	Explosive	- - - -	- - - -	2
1738	. . . .	. . . .	. . . .	Central crater eruption	Explosive + Pyroclastic Flows	- - - -	Lahars	2
1698	. . . .	. . . .	. . . .	Central crater eruption	Explosive + Pyroclastic Flows	- - - -	Fatalities, Damage, Lahars	3?
1534	06 . .	1534	07 . .	Central crater eruption	Explosive + Pyroclastic Flows	- - - -	Damage, Lahars	4
1533	10 . .	1533	11 . .	Central crater eruption	Explosive	- - - -	Lahars	2
1532	1115	. . . .	. . . .	Central crater eruption	Explosive	- - - -	Damage, Lahars?	3
1400w	. . . .	. . . .	. . . .	Central crater eruption	Explosive	Lava Flows?	- - - -	
1260w	. . . .	. . . .	. . . .	Central crater eruption	Explosive	Lava Flows?	- - - -	
1130u	. . . .	. . . .	. . . .	Central crater eruption	Explosive + Pyroclastic Flows	- - - -	- - - -	Plinian
0950x	. . . .	. . . .	. . . .	Central crater eruption	Explosive	- - - -	- - - -	
0770u	. . . .	. . . .	. . . .	Central crater eruption	Explosive	- - - -	- - - -	Plinian
0760m	. . . .	. . . .	. . . .	Central crater eruption	Explosive	- - - -	- - - -	
0740u	. . . .	. . . .	. . . .	Central crater eruption	Explosive + Pyroclastic Flows	- - - -	- - - -	Plinian
0550x	. . . .	. . . .	. . . .	Central crater eruption	Explosive	- - - -	- - - -	
0370x	. . . .	. . . .	. . . .	Central crater eruption	Explosive	- - - -	- - - -	
0180v	. . . .	. . . .	. . . .	Central crater eruption	Explosive	- - - -	- - - -	Plinian
0140s	. . . .	. . . .	. . . .	Central crater eruption	Explosive	- - - -	- - - -	Plinian
0110s	. . . .	. . . .	. . . .	Central crater eruption	Explosive	- - - -	- - - -	
0070w	. . . .	. . . .	. . . .	Central crater eruption	Explosive	- - - -	- - - -	Plinian
-0080w	. . . .	. . . .	. . . .	Central crater eruption	Explosive	- - - -	- - - -	
-0230x	. . . .	. . . .	. . . .	Central crater eruption	Explosive	- - - -	- - - -	
-1510w	. . . .	. . . .	. . . .	Central crater eruption	Explosive	- - - -	- - - -	
-2220v	. . . .	. . . .	. . . .	Central crater eruption	Explosive	- - - -	- - - -	
-2640x	. . . .	. . . .	. . . .	Central crater eruption	Explosive + Pyroclastic Flows	- - - -	Fatalities, Damage, Lahars	

Part II

VEI	Mothes, 1991		
3?	Year	Intensity	Areas Where Lahars Arrived
2			
2			
2			
2			
2			
	1914	Small	
1	1912	Small	
2			
2			
2	1906	Moderate	
3	1905	Small	
2	1903	Small	
2			
2	1886	Moderate	
2	1885	Moderate	Latacunga
2			
2			
3			
2	1880	Moderate	Information Not Available
2	1879	Small	
4	1878	Small	Information Not Available
2	1877	Large	Latacunga + Valle De Los Chillos + Rio Napa
3			
2			
2			
2			
2	1866	Moderate	Latacunga
2	1863		
2	1860		
2	1859		
2	1858		
2	1857		
2	1856	Small	Rio Napa
2			
2			
2	1854	Moderate	Latacunga
3			
2	1853	Moderate	Information Not Available
2			

2			
2			
2	1845	Small	Information Not Available
3			
4	1803	Moderate	Information Not Available
3	1768	Large	Latacunga + Valle De Los Chillos + Rio Napa
	1766	Large	Latacunga + Information Not Available
2	1758	Small	
2			
2			
4	1746	Moderate	Latacunga
2	1744	Large	Latacunga + Valle De Los Chillos + Rio Napa
4	1743	Moderate	Latacunga
3?	1742	Large	Latacunga
4	1742	Moderate	Latacunga
2	1742	Large	Latacunga
2			
3?			
4			
2	1534	Moderate	
3			
3			

Table 6: Historical eruptive frequency and associated lahar information.

(2002) is chosen here as it is the most comprehensive, detailed history for Volcán Cotopaxi.

5.2.3 Generation of the Probability Map

The final step in generating the probability map is combining the probability values reported in Table 7 with the inundation map (for flow thicknesses > 10 cm) produced from the Titan2D simulations (Figure 19).

First, the inundation files were interpolated to produce an even grid for realistic, easy interpretation. This is because the point data output by Titan2D represents a central point of the surrounding cells in the refined mesh which may be of a different size than the

VEI	Occurrence Since 1532	Run Volume Associated with VEI (m^3)	Probability of Occurrence (%)	Cumulative Probability (%)
1	1	$< 60 \times 10^4$	1.69	100
2	42	60×10^4, 10×10^5	71.2	98.3
3	10	60×10^5, 10×10^6	16.9	27.1
4	6	60×10^6, 10×10^7	10.2	10.2
5	0	$> 10 \times 10^7$	0	0

Table 7: Probability of occurrence of a particular size lahar based on association with a VEI-size eruption.

refined mesh for an adjacent point. When creating rasters at 30 m in ArcMap, this may result in inaccurate data coverage for an area, which is solved by interpolating between data points. Interpolation was done within ArcGIS using the Inverse Distance Weighted algorithm. The default settings for this algorithm were used with an output cell size chosen to match the original DEM cell size. This produced inundation areas that did not contain holes; the original grass output files contained discrete points instead of a gridded data set, so that the output is made of a series of dots rather than a continuous series of cells. This makes the raster data, which is continuous data, more appropriate for map production than the raw output reported in Figure 19.

Second, using raster calculator (a function in ArcGIS that enables the user to apply an equation to cells in raster datasets), the probability function (Equation 2, Figure 22) was applied to each layer so that each layer now represented the conditional probability of inundation. These layers were then combined with each other to produce a probability layer for lahar inundation.

This probability layer has been combined with a topographic map layer, a detailed street map layer and cadastral data to produce the final 'Map of Probabilistic Lahar Inundation for the City of Latacunga' so that the vulnerability of Latacunga can be assessed.

5.3 Map of Probabilistic Lahar Inundation for the City of Latacunga

This final map (figure 23) required four inputs to be combined in a GIS: the probability of lahar inundation layer, a topographic map, a detailed street map of Latacunga and a shapefile of cadastral data for the city.

The topographic map, a 1:50,000 topographic map with 40 m contour intervals, was scanned and georectified. The map was originally produced by the Instituto Geografico Militar (IGM), Quito in 1990.

The street map of Latacunga was provided by city authorities in the form of an AutoCAD file. This was then imported into ArcGIS and georectified using a combination of GPS data points and anchor points from the topographic map. This map provides a level of detail not available from the topographic map that is useful for vulnerability analysis.

A detailed survey of the city of Latacunga was completed using handheld GPS and included a study of the location of schools, clinics, hospitals, utilities, municipal buildings and places of population concentration (such as large factories, prisons and markets). The accuracy of these data points was tested against the topographic map and only data points with a five satellite reception were used.

The combination of these data sets allow for a detailed analysis and discussion of the vulnerability of the city of Latacunga to various scale lahars in the event of a future eruption.

The probability of inundation is calculated for each of the three VEI classes of eruptions at Cotopaxi that would likely produce lahars reaching Latacunga. The results are displayed on two maps to incorporate both the likely minimum and maximum volumes of lahars associated with these eruptions. Figure 23A shows the lower limit of expected inundations for the three VEI classes and Figure 23B shows the upper limit of inundations caused by the maximum expected volumes for each VEI class. The discussion of the vulnerability of the city of Latacunga uses the maximum limit of inundation.

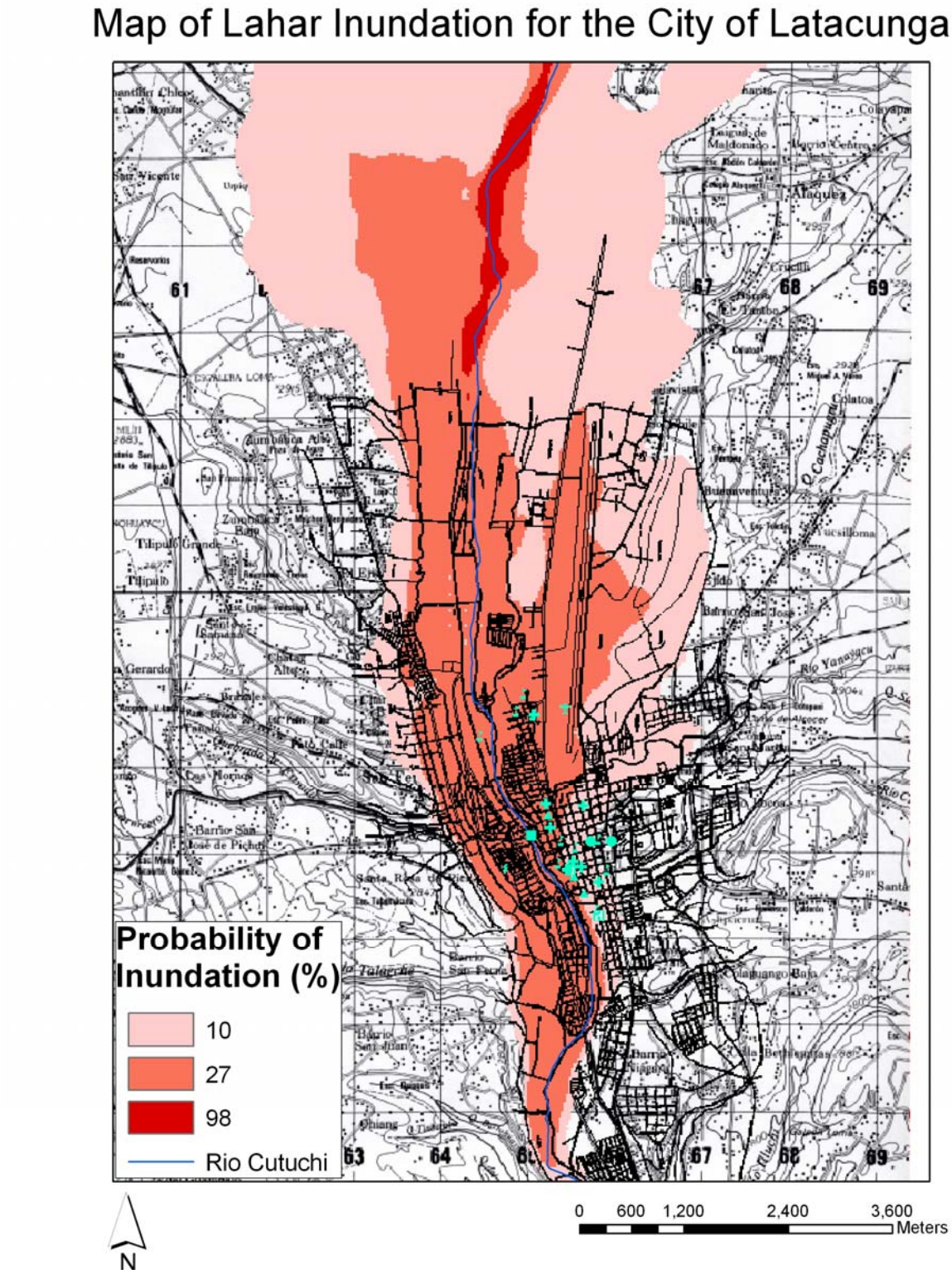

Figure 23a: Map of probabilistic lahar inundation for the city of Latacunga for the lower limit of expected volumes. Medical clinics are represented as crosses, hospitals as H's, municipal buildings as circles, schools and colleges as flags, the electric substation as a lightening bolt, the airport and military base as a airplane and places of population concentrations as triangles. A detailed look at the city center and these buildings is presented in Chapter 6.

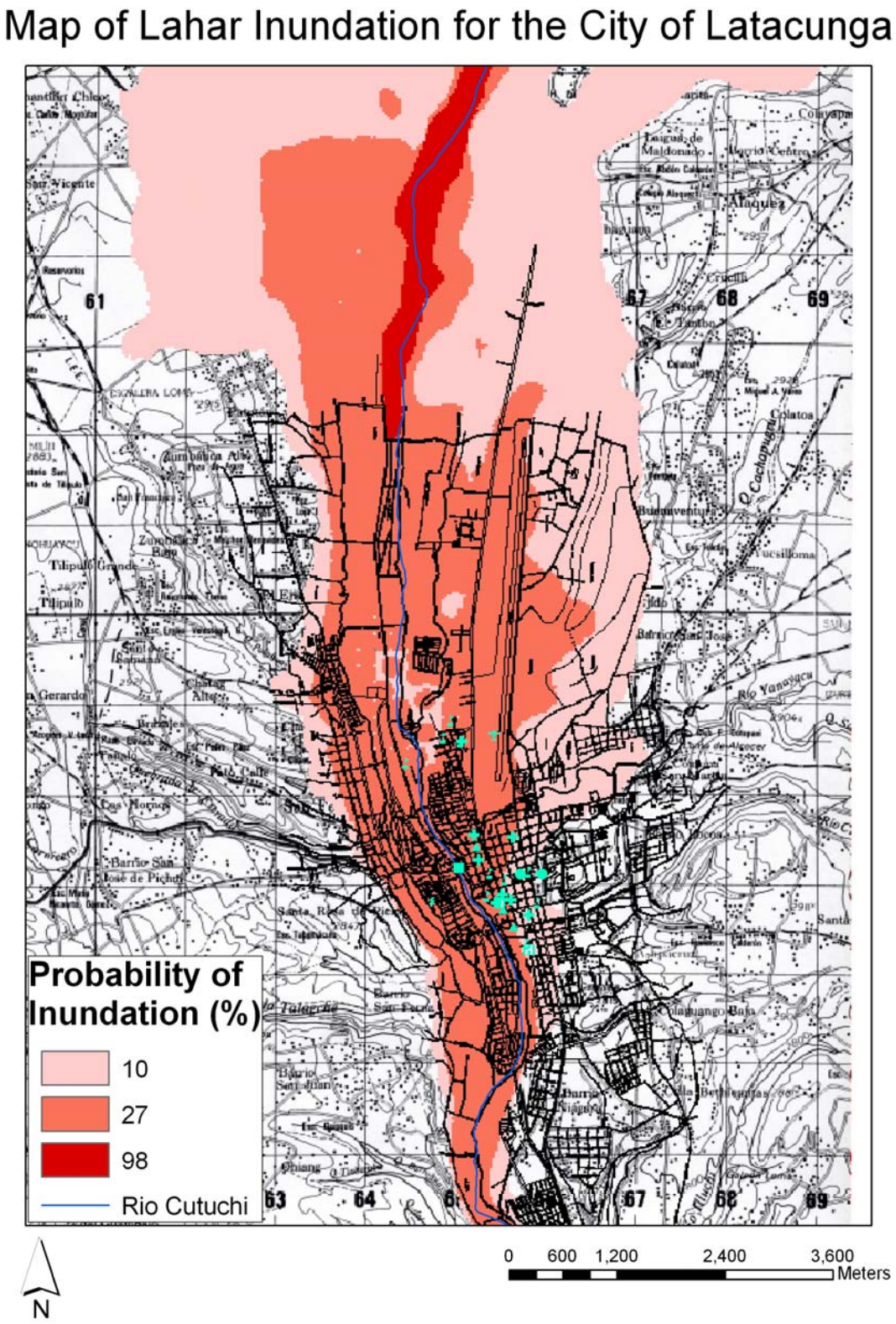

Figure 23b: Map of probabilistic lahar inundation for the city of Latacunga for the upper limit of expected lahar volumes. Symbols are the same as for figure 23a.

Chapter 6 Discussion: Assessing the Vulnerability of Latacunga

The Map of Probabilistic Lahar Inundation for the City of Latacunga provides the basis for assessing the vulnerability of the city in the event of a lahar. This map is comprises of four layers in a GIS, two of which can be queried for information on probability of lahar inundation at a point or the location of important features in the city. It is using this GIS that has enabled for the study presented here. Figure 24 shows a detailed section of this map for the city center of Latacunga.

6.1 Impact on the City of Latacunga by Large Scale Events

A large scale event is characterized by an eruption of VEI 4 or higher, as discussed in Scenario 3. This size event is similar to the 1877 eruption for which lahar volumes of 60 million m^3 and 100 million m^3 are here used. The majority of the city of Latacunga and the adjacent town of San Felipe face a 10% conditional probability of inundation if a lahar were to occur from this size eruption. Damage could be caused to most major structures including all of the schools, all of the clinics and hospitals, the military base and airport, the electric substation and the office of Civil Defense. Also affected by this inundation zone is the prison, which has a capacity for 160 prisoners and the Plaza Rafael Cajio Market which has hundreds of traders and customers every day, many of whom travel from villages across the Cotopaxi Province. These large centers of population concentration would be difficult to evacuate in an emergency.

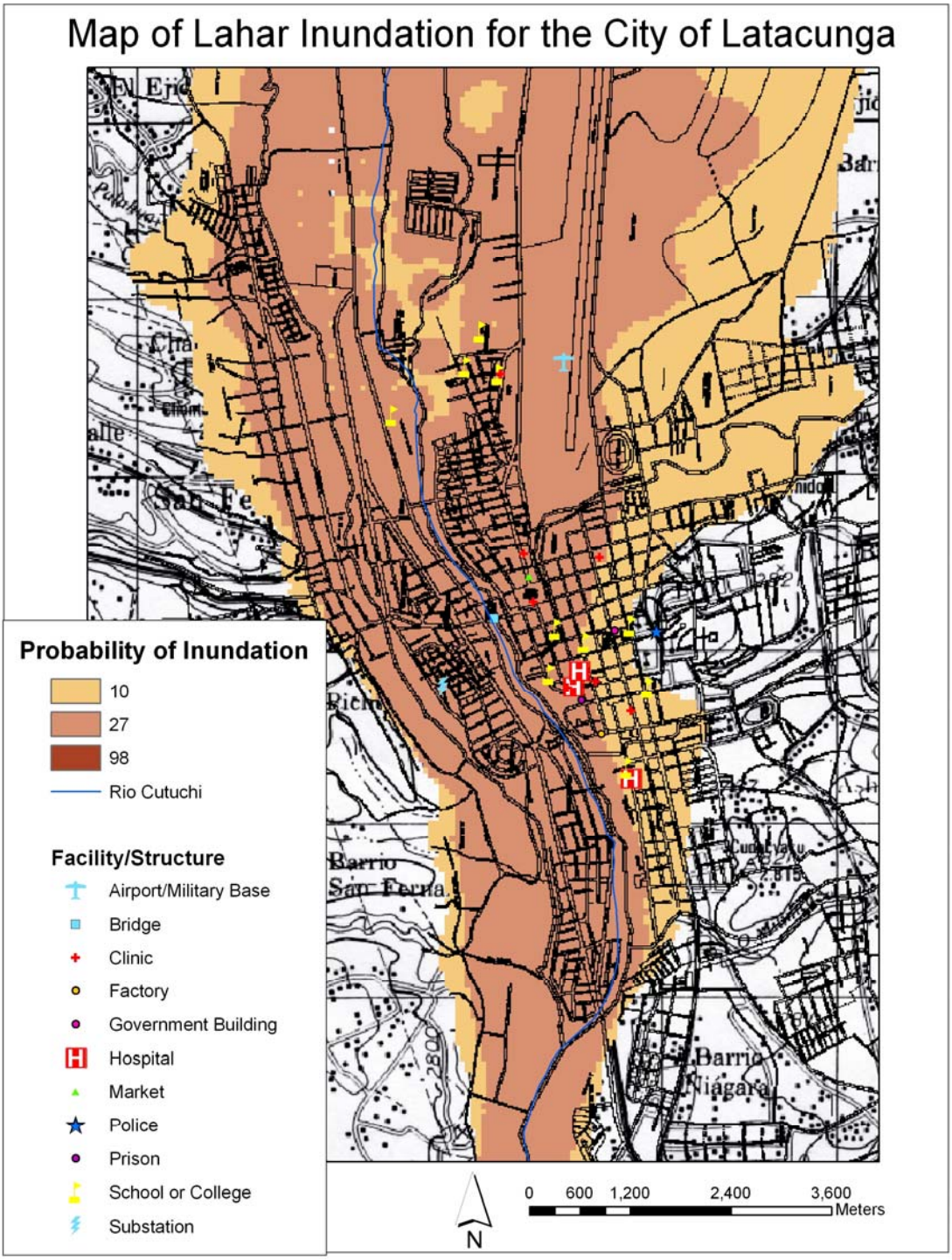

Figure 24: Detailed look at the Probabilistic Lahar Inundation map for the city centre. Maximum limits of inundations shown.

A flow of this size could have a devastating effect on the infrastructure of the city. The Pan American highway may be covered by the thickest part of the flow outside of the channel itself, inhibiting access to the city by emergency vehicles. It is likely all four bridges connecting the city could endure structural damage and would likely not be a safe route for evacuation.

The probabilistic inundation area for a large event will affect the entire business district for the city and the majority of the residential areas, endangering the lives of the 52,000 inhabitants. The widespread effect of such an inundation is important for evacuation procedures and the rescue efforts in the event of a disaster. Access to survivors would be limited due to the destruction of all major roads into the city. The ability to care for survivors would also require a substantial amount of outside assistance as all essential facilities such as electricity, medical care and the local military base are all within the 10% probability zone.

Extreme events as discussed in scenario 4 would inundate an area greater than that considered in scenario 3, but would have a conditional probability of less than 10% for inundation. The lack of occurrence of Plinian eruptions in historic times makes the probability tend towards 0%, however, reporting a 0% value would be irresponsible as it is not certain that an event of this size might never occur.

Figure 25: Bridges from the city of Latacunga across the Rio Cutuchi to the Pan American Highway. Down the left a) Bridge 5 de Julio b) Bridge Felix Valencia c) Bridge Benjamin Tepan and d) Bridge Av Ruminahui.

6.2 Impact on the City of Latacunga by Moderate Scale Events

A moderate scale event is characterized by an eruption of VEI 3, as discussed in Scenario 2. Approximately half of the city of Latacunga and the majority of the adjacent town of San Felipe faces a 27% conditional probability of inundation if an eruption of this size were to occur. Damage to 50% of the schools, the prison, 50% of the clinics and one out of the two hospitals could occur. The substation, the Pan American highway and other

major roadways could also be devastated. The southern-most bridge connecting the city (Figure 25 d) is the smallest of all of the bridges and would likely only allow small discharges to pass under and could be overtopped by a lahar of the size considered here. This would disrupt evacuation for the lower third of the City. If this bridge were to become blocked by debris, unexpected inundation may occur for larger areas than predicted due to the channel being restricted at this point. Downstream from this particular bridge is the Hospital IESS. Whilst this hospital lies just outside of the 27% probable inundation zone, it should be noted that the boarder of the grounds reach to the limits of the Rio Cutuchi (Figure 26) and therefore should also be considered at risk from a moderate event, particularly in the event of channel overbanking caused by the Av. Ruminahui Bridge.

6.3 Impact on the City of Latacunga by small scale events.

A small scale event is characterized by an eruption of VEI 1-2, as discussed in Scenario 1. It is unlikely that an eruption of this size will generate a lahar that would reach the city of Latacunga. Any flows that did reach this distal community would be small, possible hyperconcentrated stream flow and restricted to the channel or parts of the valley that are open and wide where the channel is ill-defined. An area such as this does occur to the north of Latacunga and there is a 98% chance that the areas immediately surrounding the channel will be inundated by a flow greater than 10 cm thick. This would have a minimal impact on this low population density area although some disruption may be caused to the Pan American Highway.

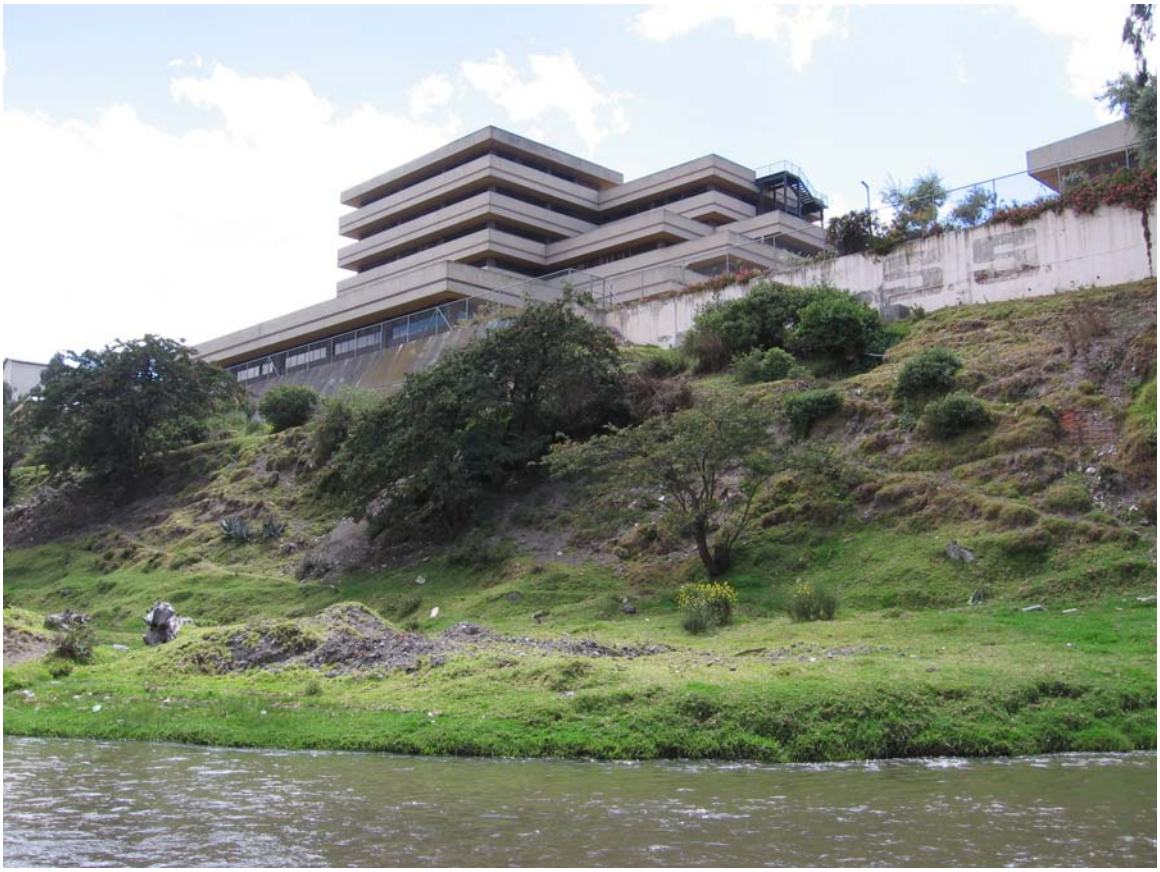

Figure 26: Hospital IESS built up to the limits of the Rio Cutuchi (in foreground).

6.4 Implications for hazard assessment

The Probabilistic Inundation Map for the City of Latacunga presented here portrays a different scenario than that displayed in the current hazard map (Hall, 2004). In reality, hazard zones are not defined by lines as they often are on classic hazard maps. Having a delineated risk zone portrays a false impression of the hazardous phenomena to the decision makers and policy holders. Is it realistic that one side of a street is at risk of destruction whilst the other is considered safe? Whilst the answer may be obvious to the volcanological community, such questions are not well handled by decision making authorities or the general public. This can either lead to a false sense of security or fear for those in designated safe or risk zones or mistrust of the maps produced and the advice

given by scientists. A probability map, such as figure 24, does not depict risk zones with lines. It presents the gradations of probability of inundation in the event of a future eruption and does not require a decision on where it is safe and where there is risk. In this way, decision making authorities and the general public are able to consider the risk they face based upon the data. They will be able to make educated decisions on whether this level of risk is acceptable for them as an individual, or as a city authority, themselves. Not only does this allow for the individual person or city to take responsibility for their own protection from hazardous phenomena, but it also relieves the scientist from shouldering that responsibility themselves. The eruptions at Montserrat (1995-present) and the legal difficulties now faced by scientists who were forced into decision making positions, has highlighted the need for this shift in responsibility (Dunkley, 2006).

With this in mind, this map provides a useful tool for considering mitigation plans for the city of Latacunga. It is clear that many of the essential resources of the city lie within the 27% probability region. The Civil Defense responsible for the city of Latacunga are preparing for an eruption in light of the recent activity at Volcán Cotopaxi. They have made plans for several 'refugios' on the high ground surrounding Latacunga and San Felipe. However, how the refugees seeking shelter at the refugios will be provided for in terms of clean water, electricity, food and medical attention is uncertain. The city is also making plans for a new hospital to be built on higher ground considered in the 'safe' zone. However, the finances for such an undertaking are limited and city authorities have relied on a land donation for the location of the new hospital. Unfortunately, the donated

plot is on the west side of the Rio Cutuchi and Pan American highway with Latacunga on the east. It is unlikely, therefore, that this new institution would be accessible for the majority of the Latacunga population.

Currently, there is no land development zoning in place for the city. Building continues in high risk areas, often without any control by the authorities. The vulnerability of the city to a lahar could be dramatically reduced by restricting building, in particular high density residential and business districts, in high risk areas. Similar land use zoning is implemented in many cities around the world, for example, the coastal region of Hilo, Hawaii is reserved for parkland only to reduce the vulnerability to tsunamis.

6.5 Conclusion

In conclusion, it is clear that an eruption greater than VEI 3 could produce lahars that would impact the city of Latacunga. There is a 27% chance that a future eruption could devastate large areas of the city including all vital resources.

This study utilized historical data, computer simulations and a detailed survey of the city of Latacunga to assess this impact and several important implications from this work have been identified. Whilst this study is very detailed and concentrated on a particular city in one drainage of Volcán Cotopaxi, the methods explored herein are transferable to other cities in the region and to other cities on volcanoes. Studies such as these require time and careful consideration and therefore should not be neglected until a time of volcanic crisis. With the increase in computational power and availability of detailed data, studies such as this will become easier in the future and will provide a key insight

into the impact of volcanological phenomena on cities located in the shadow of a volcano.

References

Aguilera, E., Pareschi, M. T., Rosi, M., Zanchetta, G., 2004. *Risk from lahars in the northern valleys of Cotopaxi Volcano (Ecuador),* Natural Hazards: 33 (2).

Andrade, D., Hall, M., Mothes, P., Troncoso, L., Eissen, J.-P., Samaniego, P., Egred, J., Ramon, P., Rivero, D., Yepes, H., 2005. *Los peligros volcánicos asociados con el Cotopaxi,* Corporación Editora Nacional*, Quito.*

Arboleda, R.A. and Martinez M, 1996. *1992 Lahars in the Pasig-Potrero River System.* In: Fire and mud: eruptions and lahars of Mount Pinatubo, Philippines, C.G. Newhall, and R.S. Punongbayan (eds), Philippine Institute of Volcanology and Seismology, Quezon City, Philippines and University of Washington Press, United States, 1115 p

Barberi, F., Macedonio, G., Pareschi, M.T., 1991. *Numerical simulation of past lahars: implication for hazard assessment.* International Conference on Active Volcanoes and Risk Mitigation, Napoli 1991. 27 August-1 September, Naples, Italy.

Barberi, F., Caruso, P., Macedonio, G., Pareschi, M.T., Rosi, M., 1992. *Reconstruction and numerical simulation of the lahar of the 1877 eruption of Cotopaxi Volcano (Ecuador).* Acta Vulcanologica 2: 35-44.

Barberi F, Coltelli M, Frullani A, Rosi M, Almeida E, 1995. *Chronology and dispersal characteristics of recently (last 5000 years) erupted tephra of Cotopaxi (Ecuador): implications for long-term eruptive forecasting.* Journal of Volcanology and Geothermal research 69: 217-239.

Costa, J.E., 1984. *Physical geomorphology of debris flows.* In: Costa, J.E. and Fleisher, P.J., eds., Developments and applications of geomorphology: Springer-Verlag, Berlin. P. 269-317.

Costa, J. E., 1988. *Rheologic, geomorphic, and sedimentologic differentiation of water floods, hyperconcentrated flows, and debris flows.* In: V. R. Baker *et al*. (eds), Flood Geomorphology, John Wiley & Sons, New York, pp. 113–122.

Costa, J.E., 1997. *Hydraulic modeling for lahar hazards at Cascades volcanoes*, Environmental & Engineering Geoscience, 3 (1).

Dunkley, P., 2006. *Problems and lessons learned at the Soufrière Hills Volcano, Montserrat.* Cities on Volcanoes 4, IAVCEI, Quito, 2006. 23 – 27 January, Quito, Ecuador.

Fread, D.M., 1988, *The National Weather Service DAMBRK Model: Theoretical background/user documentation.* Hydraulic Research Laboratory, National Weather Service, Silver Spring, MD, 320 p

Hall, M., Mothes, P., Samaniego, P., Yepes, H., Andrade, D., 2004. *Mapa regional de los peligros volcánicos potenciales del volcan Cotopaxi, Zona Sur. Esc 1:50,000.* Instituto Geofisico, Esc. Politecnica Nacional, Quito.

Iverson, R.M., 1997. *The physics of debris flows*. Reviews of Geophysics 35, 245-296.

Iverson, R.M., Schilling, S.P., Valance, J.W., 1998. *Objective delineation of lahar inundation zones*. Geol. Soc. Am. Bull. 110, 972– 984.

Macedonio, G., Pareschi, M.T., 1992. *Numerical simulations of some lahars from Mt St Helens*. Journal of Volocanology and Geothermal Research. 54: 65-80.

Major, J.J., Newhall, C.G., 1989. *Snow and ice perturbation during historical volcanic eruptions and formation of lahars and floods.* Bulletin of Volcanology. 52: 1-27.

Molina, I., Kumagai, H., Garcia, A., Nakano, M., Mothes, P., 2006. *Source process of very-long-period events accompanying long-period signals at Cotopaxi Volcano, Ecuador.* Cities on Volcanoes 4, IAVCEI, Quito, 2006. 23 – 27 January, Quito, Ecuador.

Mothes, P., 1991. *Lahars of Cotopaxi Volcano, Ecuador: Hazard and risk evaluation.* In: McCall, G.J.H., Laming, D.J.C., Scott, S.C. edits., Geohazrds: Natural and man-made. Chapman and Hall, London, pp. 53-64

Mothes, P., Hall, M., Janda, R.J., 1998. *The enourmous Chillos Valley Lahar: an ash-flow generated debris flow from Cotopaxi Volcano, Ecuador.* Bulletin of Volcanology. 59: 233-244.

Mothes, P., 2006. *Cotopaxi Volcano and the surrounding valleys*. Intra-meeting Field Trip Guide. Cities on Volcanoes 4, IAVCEI, Quito, 2006. 23 – 27 January, Quito, Ecuador.

Mothes, P., Hall, M., Andrade, D., Samaniego, P., Pierson, T., Ruiz, A.G., Yepes, H., 2006. *Character, Stratigraphy and Magnitude of historical lahars—Cotopaxi Volcano, Ecuador.* Cities on Volcanoes 4, IAVCEI, Quito, 2006. 23 – 27 January, Quito, Ecuador.

O'Brian, J.S., Julien, P.Y., Fullerton, W.T., 1992. *Two-dimensional waterflood and mudflow simulation.* Journal of Hydraulic Engineering. 119: 244-261

Patra, A.K., Bauer, A.C., Nichita, C., Pitman, E.B., Sheridan, M.F. and Bursik, M., 2005 *Parallel Adaptive Numerical Simulation of Dry Avalanches over Natural Terrain.* Journal of Volcanology and Geothermal Research 139: 1-2.

Pierson, T. C., 1980. *Erosion and deposition by debris flows at Mt.Thomas, North Canterbury, New Zealand.* Earth Surf. Processes. 5: 227–247.

Pierson, T., 1985. *Initiation and flow behavior of the 1980 Pine Creek and Muddy River lahars, Mount St. Helens, Washington.* GSA Bulletin. 96: 1056-1069

Pierson, T., Janda, R.J., Thouret, J.C., Borrero, C.A., 1990. *Perturbation and Melting of Snow and Ice by the 13 November 1985 Eruption of Nevado del Ruiz, Colombia, and Consequent Mobilization, Flow and Deposition of Lahars.* Journal of Volcanology and Geothermal Research. 41: 17-66

Pierson, T.C., Janda, R.J., Umbal, J.V., Daag, A.S., 1992. *Immediate and Long-Term Hazards from Lahars and Excess Sedimentation in Rivers Draining Mt. Pinatubo, Philippines.* U.S. Geol. Surv. Water-Resources Investigations Report 92-4039, 35p, includes map.

Pierson, T. C., and J. E. Costa, 1987. *A rheologic classification of subaerial sediment-water flows*, in Debris Flows/Avalanches:Process, Recognition, and Mitigation, Rev. Eng. Geol., vol. 7, edited by J. E. Costa and G. F. Wieczorek, pp. 1–12, Geol. Soc. of Am., Boulder, CO.

Pitman, E.B., Le L., 2005. *A two-fluid model for avalanche and debris flows.* Philosophical Transactions of the Royal Society A: Mathematical, Physical and Engineering Sciences. 363: 1471-2962

Ramon, P., Rivero, D., Boker, F., Yepes, H., 2006. *Thermal monitoring using a portable IR camera. Results on Ecuadorian volcanoes.* Cities on Volcanoes 4, IAVCEI, Quito, 2006. 23 – 27 January, Quito, Ecuador.

Rivero, D., Troncoso, L., Barba, D., Ramon, P., Yepes, H., 2006. *Anomalous activity at Cotopaxi studied with integrated seismic, thermal and visual observations.* Cities on Volcanoes 4, IAVCEI, Quito, 2006. 23 – 27 January, Quito, Ecuador.

Rodolfo, K.S., 1989. *Origin and early evolution of lahar channel at Mabinet, Mayon volcano, Philippines.* Geological Society of American Bulletin. 101: 414-426.

Rodriguez, E., C.S. Morris, J.E. Belz, E.C. Chapin, J.M. Martin, W. Daffer, S. Hensley, 2005. *An assessment of the SRTM topographic products.* Technical Report JPL D-31639, Jet Propulsion Laboratory, Pasadena, California, 143 pp.

Savage, S. B., and K. Hutter, 1989. *The motion of a finite mass ofgranular material down a rough incline.* J. Fluid Mech., 199: 177–215,.

Scott, K.M., 1988. *Origins, behavior, and sedimentology of lahars and lahar-runout flows in the Toutle-Cowlitz River system, Mount St. Helens, Washingto*n. U.S. Geological Survey Professional Paper 1447-A, 74 p

Sharp, R. P., and L. H. Nobles, 1953. Mudflow of 1941 at Wrightwood, southern California, Geol. Soc. Am. Bull. 64: 547–560.

Sheridan M.F., Bonnard C., Carreno R., Siebe C., Strauch W., Navarro M., Calero J.C., Trujillo N.B., 1999. *Report on the 30 October 1998 Rock Fall/Avalanche and breakout flow of Casita Volcano, Nicaragua, Triggered by Hurricane Mitch.* Landslide News. No 12.

Sheridan M.F., Stinton A.J., Patra A., Pitman E.B., Bauer A., Nichita C.C., 2005. *Evaluating Titan2D mass-flow model using the 1963 Little Tahoma Peak avalanches, Mount Rainier, Washington.* Journal of Volcanology and Geothermal Research 139: 89-102.

Siebert L., and Simkin T., 2002. *Volcanoes of the World: an Illustrated Catalog of Holocene Volcanoes and their Eruptions.* Smithsonian Institution, Global Volcanism Program, Digital Information Series, GVP-3, (http://www.volcano.si.edu/world/).

Sodiro, L., 1877. *Relacion sobre la erupcion del Cotopaxi acaecida el dia 26 de junio de 1877.* Imprenta Nacional, Quito, Ecuador. 40p.

Sorenson, O., W.I. Rose and D. Jaya, 2003, *Lahar hazard modeling at Tungurahua Volcano, Ecuador.* Geophysical Research Abstracts, Vol. 5, 02352.

Stinton, A.J., Sheridan, M.F., Patra, A., Dalbey, K., and Namikawa, L.M., 2004. *Integrating variable bed friction into Titan2D mass-flow model: application to the Little Tahoma Peak avalanches, Washington*, Acta Volcanologica. 16, 153-163

Tanguy, J.C., Ribiere, C., Scarth, A., Tjetjep, W.S., 1998. *Victims from volcanic eruptions; a revised database*. Bulletin of Volcanology. 60(2): 137– 144.

Takahashi, T., 1978. *Mechanical characteristics of debris flow*. J.Hydraul. Div. Am. Soc. Civ. Eng., 104: 1153–1169.

Takahashi, T., 1980. *Debris flow on prismatic open channel*. J. Hydraul.Div. Am. Soc. Civ. Eng. 106: 381–396

Vallance JW, 2000. *Lahars.* In: Encyclopedia of Volcanoes, H Sigurdsson (Ed in Chief), Academic Press, United States: pp 601.

Voight, B., 1990. *The 1985 Nevado del Ruiz volcano catastrophe: anatomy and retrospection*. Journal of volcanology and geothermal research. 44: 349—386.

Wickmann, 1976. *Markov Models for Repose-Period Patterns.* Springer-Verlag, 135-161.

Wolf, T., 1878. *Memoria sobre el Cotopaxi y su ultima erupcion acaecida el 26 de junio de 1877.* Imprenta del Comercio, Guayaquil, Ecuador. 64pp.

Censos 2001, Instituto Nacional de Estadistica y Censos, 2005 http://www.inec.gov.ec Accessed February 8th 2005, 10:14pm EST

Global Volcanism Program. http://www.volcano.si.edu/world/volcano.cfm?vnum=1502-05=&VErupt=Y&VSources=Y&VRep=Y&VWeekly=Y Accessed March 9, 2005, 9.35pm